Bimodal cell mass distribution separates CD8+ T cells into two distinct types with divergent differentiation dynamics

Jiaquan Yu[1,&], Ye Zhang[1,&*], Sarah M. Duquette[1,2], Gianfranco L. Yee[1,2], Teresa Dinter[1,3], Thomas R. Usherwood[1,4], Weida Wu[1,2], Teemu Miettinen[1], Stefani Spranger[1,3] and Scott R. Manalis[1,2,5,6*]

[1]Koch Institute for Integrative Cancer Research, Massachusetts Institute of Technology, 500 Main St building 76, Cambridge, MA 02139, USA
[2]Department of Biological Engineering, Massachusetts Institute of Technology, 21 Ames St #56-651, Cambridge, MA 02139, USA
[3]Department of Biology, MIT, Cambridge, MA, USA
[4]Harvard-MIT Department of Health Sciences and Technology, Institute for Medical Engineering and Science, Massachusetts Institute of Technology, Boston, MA, USA
[5]Broad Institute of Harvard and MIT, 415 Main St, Cambridge, MA 02142, USA
[6]Department of Mechanical Engineering, Massachusetts Institute of Technology, 33 Massachusetts Ave, Cambridge, MA 02139, USA

[&]These authors contributed equally
*Corresponding authors, yzhang23@mit.edu; srm@mit.edu

T cell heterogeneity is a cornerstone of the adaptive immune response, with CD8+ T cells playing a pivotal role in mediating cytotoxic responses to pathogens and tumors. While traditional studies have focused on phenotypic and functional diversity through surface marker expression and functional assays, the significance of biophysical properties in delineating T cell subpopulations remains underexplored. Here, we show that resting T cells exhibit a bimodal distribution in buoyant mass, which is not captured by surface marker based canonical immunophenotypes or physical parameters such as volume, density, dry mass, or light scattering. Functionally, we demonstrate that T cells with lower buoyant mass exhibit reduced proliferation, tend towards effector differentiation, and become more exhausted in the presence of innate tumor-secreted factors. Conversely, T cells with higher buoyant mass show greater memory potential and resistance to exhaustion. Our study not only provides insights into T cell biology but also suggests buoyant mass as a promising label-free biomarker to potentiate T cell-based therapies.

Understanding the potential for expansion and differentiation of CD8+ T cells is crucial for enhancing T cell-based therapies and predicting immunotherapy outcomes[1-5]. The therapeutic efficacy of T cells hinges on their capacity to proliferate[5] and resist exhaustion[6], a state of diminished function[7]. Despite considerable research on the post-activation pathways governing T cell differentiation and exhaustion[6,8], current methodologies yield limited insights into assessing the potential of CD8+ T cells prior to activation. This gap underscores the need for improved pre-activation evaluation techniques to optimize T cell-based interventions and predict their therapeutic success.

Results

In this context, buoyant mass measurement using Suspended Microchannel Resonator (SMR) technology emerges as a particularly promising tool. SMR has demonstrated unparalleled precision in measuring the buoyant mass of individual cells[9,10], offering insights into cellular states beyond traditional biochemical markers[11,12]. Previous studies have correlated buoyant mass with T cell proliferation, notably distinguishing proliferating from non-proliferating cells[13]. Here, we used the SMR to measure buoyant mass of naive, unactivated CD8+ T cells and observed a bimodal distribution consisting of "light" (ranging from 5 to 7.5 pg in mice and 5 to 10 pg in humans) and "heavy" (exceeding 7.5 pg in mice and 10 pg in humans) cells (**Fig. 1a, b**). The bimodal distribution is reproduced across 38 independent experiments on mouse spleen samples and 7 human PBMC samples. Notably, we observed a species-specific variance in the light/heavy ratio: in mice, the light T cell populations constituted 4-9%, whereas in humans, they accounted for 10-13% (**Fig. 1c**). This bimodality was unexpected and suggests a deeper complexity in T cell physiology.

We next sought to determine if the light and heavy populations could be distinguished by light scattering measurements on conventional flow cytometry, which are commonly used to differentiate cell populations

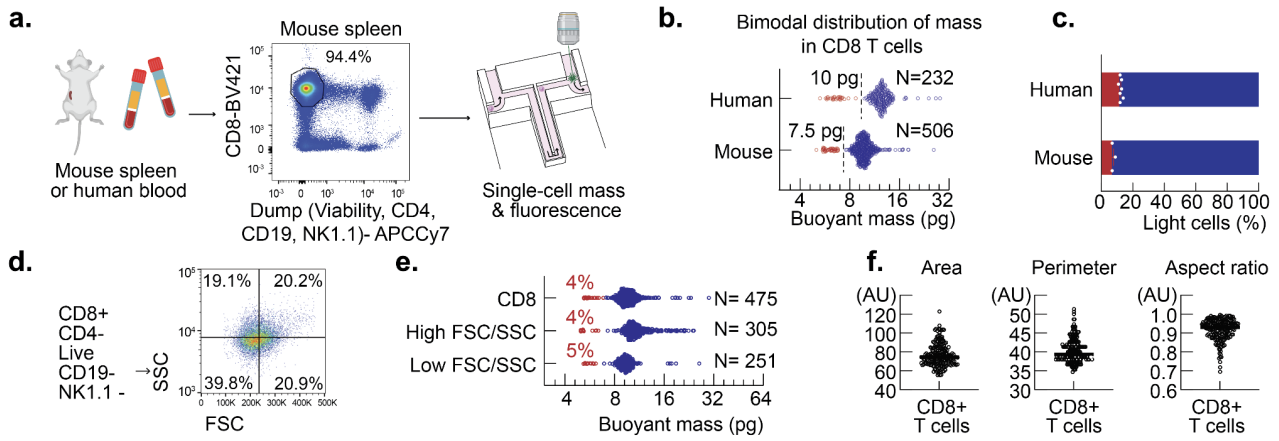

Fig. 1 | Mouse and human CD8+ T cell samples consistently exhibit a bimodal buoyant mass distribution. a, Schematic of the workflow for sorting CD8+ T cells from either mouse spleen or human PBMC samples by flow cytometry for measurements using the fluorescent coupled SMR for single-cell mass profiling and fluorescent pairing. **b**, Mass distribution of mouse and human CD8+ T cell samples displaying light (5-7.5 pg in mice, 5-10 pg in humans) in red and heavy (>7.5 pg in mice, >10 pg in humans) in blue. **c**, The percentage of light (red) and heavy (blue) T cells within a CD8+ T cell sample for mouse (n=3) and human (n=7) samples. Mean ± s.e.m. are shown. **d**, FSC vs SSC gating of mouse CD8+ T cells on flow cytometry. High FSC/SSC (upper right) and low FSC/SSC (lower left) were sorted for SMR measurements. **e**, Mass distribution of CD8+ T cells and CD8+ T cell populations sorted by FSC/SSC. **f,** Measurements of total cell area, perimeter, and aspect ratio of mouse CD8+ T cells on the Amnis® Imaging Flow Cytometer.

based on cell size (forward scatter, FSC) and granularity or internal complexity (side scatter, SSC)[14,15]. T cells from a mouse spleen sample form a single concentrated cluster when plotted by FSC and SSC (**Fig. 1d**), indicating homogeneity in cell size and granularity. Furthermore, to ascertain whether the light and heavy T cell populations could be enriched by light scattering, we evenly divided the cluster into four quadrants and sorted high FSC/SSC (upper right) and low FSC/SSC (lower left) (**Supplementary Fig.1**) for buoyant mass measurement (**Fig. 1d**). Interestingly, cells from both quadrants contained light and heavy populations (**Fig. 1e**). Though cells from the high FSC/SSC quadrant had relatively greater mass in the heavy population, likely due to the presence of larger granular cells, the light T cells exhibited similar mass profiles across both quadrants. In addition to light scattering, we also analyzed mouse spleen T cells by imaging flow cytometry and did not observe a bimodal distribution based on assessments from brightfield images of total cell area, perimeter, and aspect ratio measurements (**Fig. 1f**, **Supplementary Fig.2**). Thus, light and heavy T cell populations are indistinguishable by routinely used methods such as light scattering and microscopy.

Since buoyant mass depends on cell volume and buoyant density, which in turn depend on dry volume and dry density, respectively[16,17], we utilized an established method to measure these additional biophysical parameters (**Supplemental Note 1**). Remarkably, naive CD8+ T cells isolated from both mouse spleen and human PBMC show an overlap of light and heavy for both volume and buoyant density, indicating that neither volume nor buoyant density alone accounts for the bimodality observed in T cell buoyant mass (**Fig. 2a**). Yet, when plotting buoyant density versus volume for each individual cell, the two distinct populations are readily apparent, as anticipated by the iso-buoyant mass contour (dashed line). Similarly, the light and heavy populations also overlap in terms of dry volume and dry density (**Fig. 2b**), yet when plotted versus each other, the two populations are distinct. In contrast, the iso-dry mass contour reveals overlap between these two populations. This is more readily apparent when dry mass is plotted versus buoyant mass, showing clear bimodality for the latter but not the former. Cell dry mass has long been used as a metric for cell growth because it integrates all cellular components, including protein, nucleic acid, and lipid content. Although, in prior growth studies buoyant and dry mass generally lead to similar qualitative conclusions, they reflect fundamentally different properties of the cell. For cells in media where the density is close to that of water, the relationship between the cell's buoyant and dry mass is governed by its dry density (**Supplemental Note 1**). This divergence in buoyant and dry mass measurements reveals molecular composition differences between the heavier and lighter T cells, suggesting that a functional examination of these populations could provide deeper insights into T cell behavior.

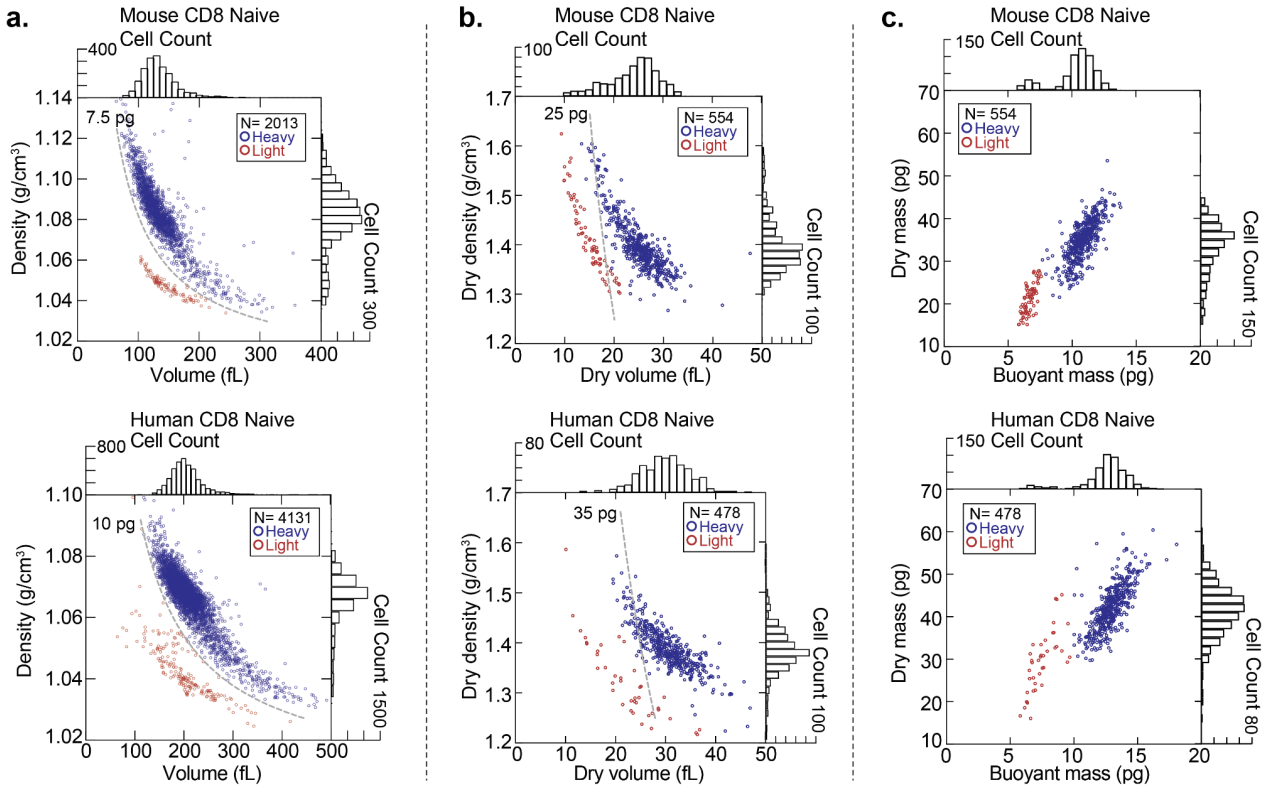

Fig. 2 | Light and heavy T cells are uniquely distinguishable by buoyant mass. a-c, Scatter plot of (**a**) density (g/cm^3) vs volume (fL) (dashed line indicates iso-buoyant mass), (**b**) dry density (g/cm^3) vs dry volume (fL). (dashed line indicates iso-dry mass), and (**c**) dry mass (pg) vs buoyant mass (pg) for naïve CD8+ T cells from either mouse spleen or human PBMC samples.

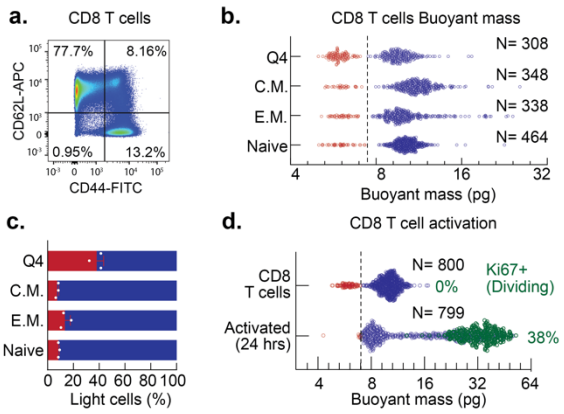

Fig. 3 | Bimodal buoyant mass distribution in CD8+ T cells is not defined by canonical differentiation or activation states. a, Flow cytometric sorting of CD8+ T cell samples by their CD44 and CD62L expression. **b**, Buoyant mass profiles of naive (CD44-,CD62L+), central memory (CM, CD44+,CD62L+), effector memory (EM, CD44+,CD62L-), and quadrant 4 (Q4, CD44-/CD62L-) T cells. Color indicates mass subpopulation with light in red and heavy in blue. **c**, The percentage of light (red) and heavy (blue) T cells within the four CD8+ T cell subpopulations (n=3). Mean ± s.e.m. are shown. **d**, Buoyant mass profiles of CD8+ T cells before activation and after 24 hrs of activation. Cells actively expressing Ki67 at the time of measurement are indicated in green.

To determine whether heavy or light T cells are associated with a particular differentiation state, we followed a conventional protocol to sort live CD8+ T cells from mouse spleen samples into subpopulations of naïve (CD44-, CD62L+), central memory (CD44+, CD62L+), effector memory (CD44+, CD62L-), and Q4 (CD44-, CD62L-) T cells based on their expression of surface markers CD44 and CD62L[18,19](**Fig. 3a, Supplementary Fig.3**). Mass profiling of T cell subpopulations uncovered the presence of both light and heavy T cells within each category (**Fig. 3b**), indicating a persisting bimodal distribution throughout different T cell differentiation stages and stable across replicates (**Fig. 1f**). Notably, the Q4 population, a rare and less differentiated state of T cells[18,20], contained the most substantial percentage of light T cells (exceeding 30%, **Fig. 3c**). However, due to the small overall size of the Q4 population, these light T cells translate to less than 2% of the total T cell population. To determine whether light or heavy T cells are indicative of cell proliferative state, we activated mouse spleen CD8+ T cells in vitro with anti-CD3/CD28[21,22]. T cells were allowed to grow for 24 hours, then stained with the proliferation marker Ki67 and measured with the fluorescent coupled SMR (**Fig. 1a**). As previously reported, activated T cells increase buoyant mass to up to 60 pg (**Fig. 3d**)[13], with 38% of

them positive in Ki67, which indicates an active dividing status[23]. Importantly, no Ki67 positive cells were captured prior to activation and all Ki67+ dividing T cells after activation reside in the >12 pg buoyant mass region which exceeds the heavy population range, suggesting that the bimodal distribution is independent from proliferative events.

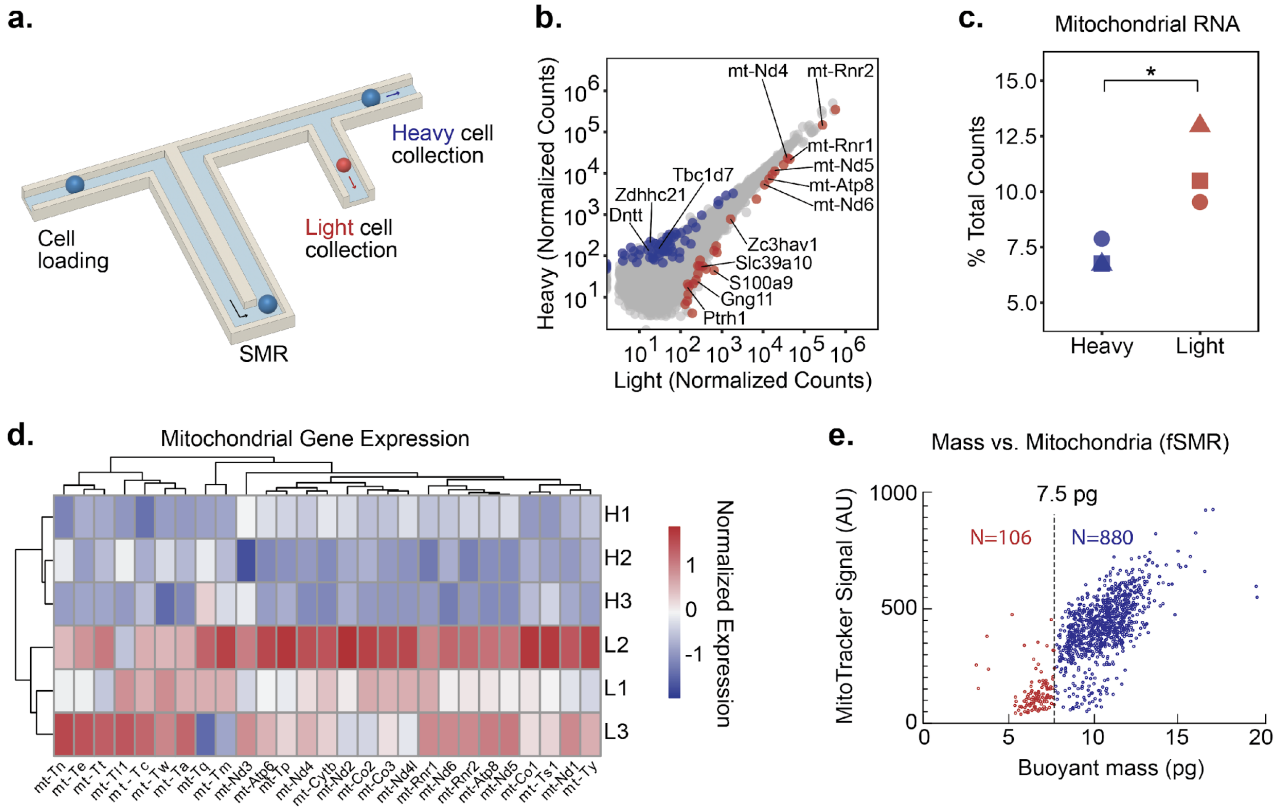

Fig. 4 | Light T cells have higher fractional mitochondria RNA yet lower MitoTracker deep red FM signal than heavy T cells. a, Schematic of mass-based single-cell sorting platform via SMR for subsequent transcriptional and functional analysis. The sorting accuracy is over 98%. **b,** Normalized gene counts for heavy and light T cells. Differentially expressed genes are colored (adjusted p-value ≤ 0.05 and absolute fold change ≥ 1.5). Blue denotes upregulation in heavy cells, and red denotes upregulation in light cells. **c**, Comparison of the percentage of total mitochondrial RNA (unpaired t-test, p-value = 0.049). **d**, Heatmap of normalized counts for all expressed mitochondrial genes. Hierarchical clustering (complete, Euclidean distance) is performed on samples and genes. **e**, MitoTracker deep red FM fluorescent signal vs buoyant mass (pg) measured for CD8+ T cells.

Light and heavy naive T cells differ in respiring mitochondrial content.

To investigate the difference between the light and heavy populations, we developed a single-cell sorting platform that utilizes the SMR to separately collect light cells and heavy cells based on buoyant mass (**Fig. 4a**). This platform consists of one cell loading channel and two sorting channels, which are controlled by three independent pressure regulators (**Supplementary Fig.4, Supplementary Fig.5**). Light and heavy naive CD8+ T cells from 3 mice were sorted for bulk RNA-sequencing (RNA-seq). We performed differential expression analysis (padj<0.05, log2FC>1.5) and identified 102 differentially expressed genes (DEGs) (**Fig. 4b, Supplementary Fig.6**). However, gene set enrichment analysis yielded no enriched pathways (FDR<0.05) (**Supplementary Fig.7**), and specifically no significant differences were found in pathways associated with cell apoptosis, autophagy, mitophagy, or cell cycle between light and heavy populations (**Supplementary Fig.8**). Furthermore, principal component analysis (PCA) across all libraries revealed that light and heavy samples do not separate across any PC loadings (**Supplementary Fig.9**). Intriguingly, highly expressed DEGs (>104) were dominated by mitochondrial transcripts, with 8 highly expressed DEGs, 6 of which originated from the mitochondrial genome (**Fig. 4b**). Having observed this striking difference, we analyzed the percent of mitochondrial RNA within each library. This revealed that light cells have 3.9% more mitochondrial RNA than heavy cells (p-value = 0.049) (**Fig. 4c**). Notably, we further confirmed that every mitochondrial gene was upregulated in light cells and samples successfully formed light and heavy clusters by plotting all mitochondrial genes in a heatmap (**Fig. 4d**). To investigate mitochondrial content beyond the transcriptome, CD8+ T cells were stained with MitoTracker deep red FM, which is a dye that targets respiring mitochondria

in live cells[24]. We simultaneously measured single-cell mass and MitoTracker deep red FM fluorescent intensity using the fluorescence coupled SMR platform. Although we observed increased fractional mitochondrial mRNA content in light T cells compared to those in the heavy, the total respiring mitochondrial content as represented by MitoTracker deep red FM in light T cells is lower (**Fig. 4e**).

Light T cells are more likely to remain effector during activation.

Mitochondrial activity governs the metabolic capacity of T cells and is critical in T cell activation and differentiation[25, 26]. Specifically, impaired mitochondrial function has been shown to limit T cell proliferation and function upon persisting antigen stimulation[27]. Given light cells have elevated mitochondrial mRNA but lower mitochondrial content (**Fig. 4e,f**), we hypothesized that following activation, the light T cells will be impaired in their ability to proliferate and develop. To determine this, we adapted and optimized a protocol to activate approximately 200 T cells sorted by buoyant mass in distinct microwells with anti-CD3/28 beads[28] (**Fig. 5a**). During the initial two days of activation, both light and heavy T cells formed compact clusters of similar sizes, suggesting comparable migration and aggregation capabilities (**Fig. 5b, Supplementary Fig.10**). Expansion of the clusters began on the second day for both groups; however, by the third day, the heavy T cells exhibited larger cluster sizes than their counterparts (**Fig. 5b, Supplementary Fig.10**). This proliferative advantage for heavy T cells resulted in a notably higher cell count by day 6 (**Fig. 5C**). As observed following activation of unsorted T cells (**Fig. 3d**), both light and heavy sorted populations accumulated buoyant mass by day 6, indicating that although light cells are not as proliferative as heavy cells, they are still able to accumulate similar amounts of biomass (**Supplementary Fig.11**).

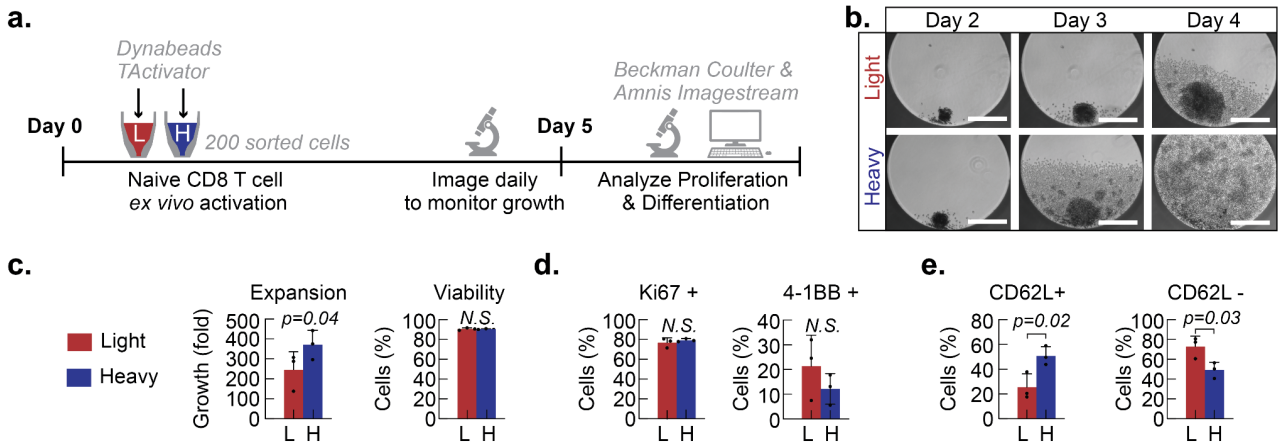

Fig. 5 | Light and heavy T cells both activate with diverging differentiation capacity. a, Customized T cell activation protocol to activate 200 T cells for marker analysis on day 6. **b**, Brightfield images of T cells during activation on days 2, 3, and 4. Scale bar is 300 um. **c**, Bar plot of total cell expansion calculated by the fold change of cell counts on day 6 to the number of cells seeded plotted for light and heavy. Percent of cells viable on day 6 of activation plotted for light and heavy. **d-e**, Analysis via Amnis imagestream to analyze (**d**) Ki67, 4-1BB, and (**e**) CD62L expression on day 6 of activation. (**c**) (**d**) & (**e**) Data are shown as mean ± s.e.m., representative of three independent experiments. Statistical analysis was performed using two-tailed unpaired t-tests with Welch's correction.

Having observed that both light and heavy populations are capable of expansion, we next evaluated their differentiation tendencies using the Amnis imaging flow cytometer. We first confirmed that both populations exhibited a similar percentage (>85%) of live (**Fig. 5c**), proliferative (Ki67+), and costimulatory (4-1BB+) cells (**Fig. 5d**) on day 6, suggesting comparable viability and fitness once activated. Interestingly, heavy cells were more likely than light cells to be CD62L positive (**Fig. 5e**). Given that almost all T cells expressed CD44 at this activation stage (**Supplementary Fig.12**), CD62L presence signifies a lymphoid homing (central memory) phenotype (CD44+,CD62L+), whereas its absence suggests an effector phenotype (CD44+,CD62L-) (**Fig. 5e**). These findings imply a predilection of heavy T cells for memory formation, contrasting with the tendency of light T cells towards effector differentiation.

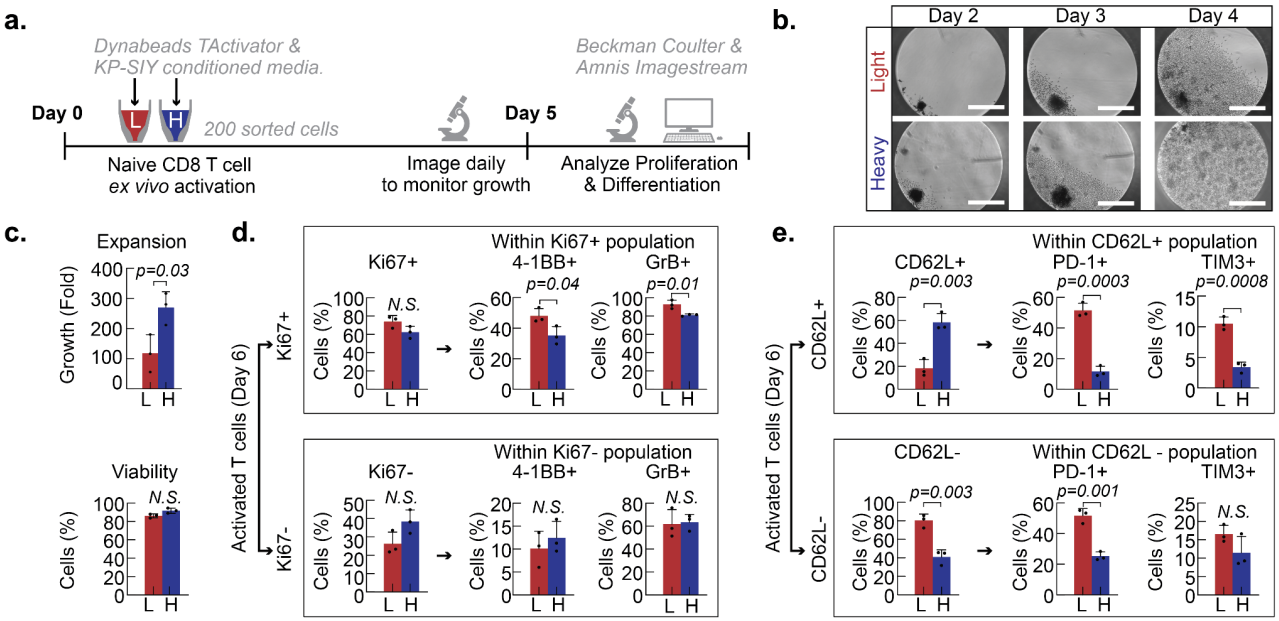

Fig. 6 | Light and heavy T cells respond differently during activation in tumor conditioned media. a, Customized T cell activation protocol to activate 200 T cells in KP-SIY tumor conditioned media for marker analysis on day 6. **b**, Brightfield images of T cells during activation on days 2, 3, and 4. Scale bar is 300 um. **c**, Bar plot of total cell expansion calculated by the fold change of cell counts on day 6 to the number of cells seeded plotted for light and heavy. Percent of cells viable on day 6 of activation plotted for light and heavy. **d**, Amnis Imagestream analysis of Ki67 expression and expression of granzyme B and 4-1BB within both Ki67+ and Ki67- populations on day 6 of activation. **e**, Amnis Imagestream analysis of CD62L expression and expression of T cell exhaustion markers TIM3 and PD-1 within the CD62L+ and CD62L- populations on day 6 of activation. (**c**) (**d**) & (**e**) Data are shown as mean ± s.e.m., representative of three independent experiments. Statistical analysis was performed using two-tailed unpaired t-tests with Welch's correction.

Light T cells are related to exhaustion.

In addition to influencing the renewal and differentiation of T cells, mitochondrial dysfunction has also been linked to T cell exhaustion in the context of tumor responding T cells[27,29]. Specifically, depolarized or dysfunctional mitochondria has been reported as a marker for CD8 terminal exhaustion in vivo[30] and in vitro[31]. The use of tumor-conditioned media is a well-established method for in vitro T cell differentiation to induce exhaustion[32]. In our study, we used the KP-SIY lung tumor cell line[33, 34], known for inducing T cell exhaustion[35] to generate KP-SIY tumor conditioned media. We adapted the same low cell count activation protocol (**Fig. 5a**), and replaced T cell activation media with 10% of the conditioned media (**Fig. 6a**). Both T cell populations were able to form clusters and expand (**Fig. 6b, Supplementary Fig.13**), with the light population growing significantly slower than the heavy population at day 6 (**Fig. 6c**). To further explore potential differences in viability or differentiation potential, flow-imaging analysis was performed on the Amnis ImageStream system (**Supplementary Fig.14**). There were no significant differences between light and heavy populations in day 6 viability or proliferation (Ki67+). Within the proliferating population (Ki67+), larger proportions of light cells exhibited expression of costimulatory surface marker 4-1BB (**Fig. 6d**), indicating a stronger inflammatory response toward the conditioned media[36]. No significant differences were observed in the non-proliferating population (Ki67-) (**Fig. 6d**) or cytotoxicity marker granzyme B (GrB). Consistent with activation experiments without conditioned media, we observed differences in maturation of the light and heavy T cells, as evidenced by CD62L expression with heavy preferring to differentiate into the lymphoid homing (central memory) phenotype (CD62L+) and light preferring to differentiate into an effector phenotype (CD62L-), indicating a robust and intrinsic distinction in maturation commitment between the light and heavy T cells (**Fig. 6e**). Furthermore, within both the CD62L positive and negative populations, the light T cell lineage was more prone to exhaustion as indicated by PD-1+ than the heavy T cells (**Fig. 6e**). Within the lymphoid homing (central memory) phenotype, the critical population for antitumor immune response [37,38], light populations are significantly more likely to be terminally exhausted (PD-1+, TIM3+) than their counterparts, suggesting their blunted ability to form memory.

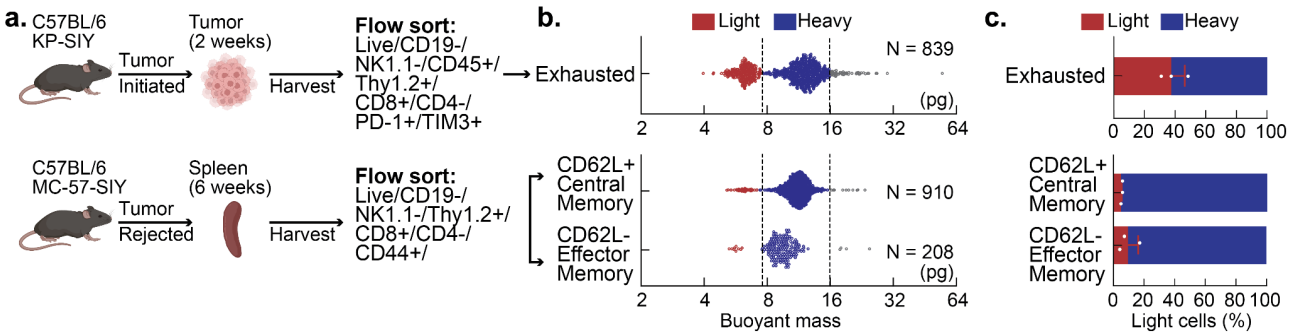

Fig. 7 | Light T cells are enriched in tumor infiltrating exhausted T cells. a, Protocol to generate a KP-SIY tumor to obtain tumor infiltrating exhausted T cells in vivo. Exhausted T cells are sorted from the tumor 2 weeks after injection. Protocol to generate central memory and effector memory T cells in vivo with the MC-57-SIY model, where the tumor does not engraft. Central and effector memory T cells are sorted from the spleen 6 weeks after injection. **b**, Mass profiles of sorted cell populations. Points colored by mass with light(<7.5 pg) in red and heavy(>7.5 pg) in blue. **c,** The percentage of light (red) and heavy (blue) T cells for sorted cell populations for 3 independent replicates. Mean ± s.e.m. are shown.

Having established a correlation between light cells and their propensity for exhaustion when activated in KP-SIY tumor conditioned media, we embarked on an investigation to determine if this is observed in vivo as well. Tumor infiltrating T cells were isolated from subcutaneous KP-SIY tumors on day 14 following tumor inoculation as previously published[35]. Exhausted T cells among the tumor infiltrating T cells were identified using Live/dead-, CD45+, Thy1.2+, CD8+, CD4-, PD-1+ and TIM3+ (**Fig. 7a, Supplementary Fig.15**). As anticipated, the infiltrating exhausted T cells exhibited a bimodal distribution with a higher percentage of light cells compared to CD8 or naive (CD62L+,CD44-) populations (**Fig. 7b**). To corroborate our ex vivo observation that light T cells are impaired for memory cell development, we performed in vivo central memory and effector T cells enrichment experiments, using a MC57-SIY model [39]. In this model, tumors are spontaneously rejected in a CD8+ T cell dependent manner[40], resulting in the induction of memory T cell populations. After 6 weeks, these central and effector memory T cell populations were sorted from the spleen (**Supplementary Fig.16**). These data supported our earlier findings: light cells were significantly depleted in the central memory population (**Fig. 7c**) compared to the naive population of healthy mice (**Fig. 3c**). These results suggest a synergistic coexistence between the biophysical phenotype and cellular differentiation mechanisms, further highlighting the intricate interplay between T cell phenotypes and their functional outcomes.

Discussion

Buoyant mass emerges as a unique marker for delineating light and heavy T cells. To our knowledge, the SMR is currently the only tool capable of directly measuring buoyant mass with high precision, setting it apart from standard chromatography-like methods like gravitational Field-Flow Fractionation (FFF), which relies on the ratio of buoyant mass to cell radius[41,42]. A limitation of our methodology is that the SMR sorting approach can only handle up to a few hundred cells per hour — falling short of the needs for comprehensive downstream mechanistic investigations. Overcoming this bottleneck will require further technical innovation. Increased throughput would not only bolster mechanistic studies, but it would also facilitate the introduction of light cell populations into RAG-1 knockout lymphocyte deficient mice to ascertain if a correlation exists with T cell dysfunction under immune checkpoint inhibitor treatment. This correlation could potentially act as a predictive marker for patient outcomes. Moreover, higher throughput would allow for intricate molecular experiments, especially pertaining to mitochondria, to further our understanding of the link between buoyant mass and mitochondrial function. Another area for improvement is the temporal resolution of our measurements; T cell buoyant mass has only been assessed at a singular timepoint. Developing new methods for longitudinally tracking individual cells and their lineages will enable us to map out their developmental pathways and pinpoint the precise phases in hematopoiesis at which light and heavy T cells are formed.

Methods

Mice. All mice used in **Figs. 1-6** were bred and maintained under specific pathogen-free conditions at the Koch Institute Animal facility. Animal procedures were approved by the Massachusetts Institute of Technology Committee on Animal Care (CAC), Division of Comparative Medicine (DCM). Animals were housed on hardwood chip bedding, with a 12/12 hour light-dark cycle at a temperature of 70°F +/– 2 and humidity of 30–70%. These mice were maintained on a mixed C57BL/6; 129/Sv background. Mice were 12-20 weeks old at the time of experimentation, unless otherwise described.

All mice used in **Fig. 7** were of a C57BL/6 background. C57BL/6 mice were purchased from Taconic (Strain #B6NTac) or Jackson Laboratories (Strain #000664). Mice were 6-12 weeks old at the time of experimentation, unless otherwise described.

Mouse Spleen processing. Mice were euthanized via CO_2 asphyxiation. The spleen was removed and mashed through a 70 um filter to create a single cell suspension. The spleen sample was then enriched for CD8+ T cells via the EasySep Mouse CD8+ T cell Isolation Kit (StemCell, 19853) following the manufacturer's protocol. The CD8+ T cell enriched sample was then stained with FC Block (101302), eBioscience Fixable Viability Dye (APC-Cy7, 65-0865-14), CD19 (APC-Cy7, 47-0193-80), CD4 (APC-Cy7, 47-0042-80), NK1.1 (APC-Cy7, 47-5941-80), CD8 (BV421, 100725), CD62L (APC, 17-0621-81), and CD44 (FITC, 11-0441-81) for fluorescent activated cell sorting of CD8+ T cells and T cell subpopulations.

Human PBMC processing. Apheresis leukoreduction collars from anonymous healthy platelet donors were obtained from the Brigham and Women's Hospital Specimen Bank under an Institutional Review Board–exempt protocol. Human peripheral blood mononuclear cells (PBMCs) were isolated via density gradient centrifugation (Lymphoprep, StemCell Technologies Inc, 07801). PBMC samples were then stained with FC Block (422301), eBioscience Fixable Viability Dye (APC-Cy7, 65-0865-14), CD19 (APC-Cy7, 363009), CD4 (APC-Cy7, 47-0049-41), CD56 (APC-Cy7, 47-0567-41), CD14 (APC-Cy7, 47-0149-41), CD8 (APC, MHCD0821), CD197(CCR7) (PE, 353203), and CD45RA (PE-Cy7, 25-0458-42) for fluorescent activated cell sorting of CD8+ T cells.

T cell buoyant mass measurement using SMR. Single-cell buoyant mass was measured using the SMR as previously described[9]. The SMR is a cantilever-based mass sensor with an embedded microfluidic channel. As a cell flows through the channel along the cantilever, the change in resonance frequency detected corresponds to the buoyant mass of the cell. Full measurement details can be found in Ref. [9]. Prior to a set of measurements, the SMR was cleaned with 0.05% Trypsin-EDTA (Invitrogen, 25300054) for 20 min, followed by 5% bleach for 3 min and then a 5-min rinse with DI-H_2O, to remove persistent biological debris. After cleaning, the SMR was passivated with 1 mg/mL PLL-g-PEG (Nanosoft Polymers, SKU#11354) in H_2O for 10 min at room temperature, followed by a 5-min rinse with Flow Cytometry (FACS) Staining Buffer (Rockland, MB-086-0500). All measurements were carried out in FACS buffer at room temperature for no more than 30 minutes. The SMR was briefly washed with the FACS buffer between each sample.

During the measurement, all the samples were loaded into the SMR through 0.005-inch-inner-diameter fluorinated ethylene propylene (FEP) tubing (Idex, 1576L). The fluid flow across the SMR was driven by three independent electronic pressure regulators (MPV1, Proportion Air) and three solenoid valves (S070, SMC). A consistent differential pressure was applied across the SMR to maintain constant shear and data rate for cell measurement. All the regulators, valves and data acquisition were controlled by custom software coded in LabVIEW 2020 (National Instruments).

T cell density and volume measurement. Cell density and volume were measured using fluorescent exclusion techniques as previously described. To couple single-cell mass and volume measurements, a fluorescent microscope was positioned at the entry to the SMR cantilever. The fluorescence level emitted from the detection region was continuously monitored by a photomultiplier tube (PMT, Hamamatsu, H10722-20). Cells were suspended in PBS +2%FBS with 5 mg/mL FITC-conjugated dextran (Sigma, FD2000S-250MG). When no cell was present at the detection region, the PMT detected a high fluorescence baseline from the fluorescence buffer. As a cell passed through, the fluorescence signal decreased proportionally to the volume of the cell. Immediately after the volume measurement, each single cell flowed through the SMR cantilever and the corresponding buoyant mass was measured.

Buoyant mass is given by

$$m_b = V(\rho - \rho_{fluid}) = m(1 - \frac{\rho_{fluid}}{\rho}) \quad (1)$$

where V is the volume of the cell, m is the total mass and ρ is the density of the cell immersed in a fluid of density ρ_{fluid}. The fluid density of PBS +2%FBS with 5 mg/mL FITC-conjugated dextran is 1.005 g/cm^{-3}. Cell density ρ is then computed using equation (1).

T cell dry mass measurement. Cell dry mass and dry density were calculated from SMR measurements as previously described[16]. The relationship between buoyant mass and dry mass is given by

$$m_b = m_{dry}(1 - \frac{\rho_{fluid}}{\rho_{dry}}) \quad (2)$$

where ρ_{fluid} is the density of the fluid that the cell is immersed in. To measure dry mass and dry density, the two bypass channels on either side of the SMR cantilever were filled with different fluids, one with an H_2O-based PBS solution, and the other with a D_2O-based PBS solution (Sigma, 151882-1KG). Two consecutive buoyant mass measurements were taken of individual T cells; the first was taken with the cell immersed in the H_2O-based solution, and after a brief period of stopped flow for the intracellular H_2O to exchange to D_2O, the second was taken with the cell immersed in a D_2O-based PBS solution. Given the density difference between H_2O and D_2O and the intracellular fluid exchange between the two buoyant mass measurements, equation (1) in these two cases yields

$$m_{b_{fl1}} = m_{dry}(1 - \frac{\rho_{fl1}}{\rho_{dry}}) \quad (3)$$

$$m_{b_{fl2}} = m_{dry}(1 - \frac{\rho_{fl2}}{\rho_{dry}}) \quad (4)$$

where $m_{b_{fl1}}$ and $m_{b_{fl2}}$ are measured buoyant mass of the cell immersed in H_2O-based PBS solution (ρ_{fl1}=1.005 g/cm^{-3}) and D2O-based PBS (ρ_{fl2}=1.005 g/cm^{-3}) respectively. Dry mass and dry density of the cell can be calculated by

$$m_{dry} = \frac{m_{b_{fl1}} \cdot \rho_{fl2} - m_{b_{fl2}} \cdot \rho_{fl1}}{\rho_{fl2} - \rho_{fl1}} \quad (5)$$

$$\rho_{dry} = \frac{m_{b_{fl1}} \cdot \rho_{fl2} - m_{b_{fl2}} \cdot \rho_{fl1}}{m_{b_{fl1}} - m_{b_{fl2}}} \quad (6)$$

Mitochondrial staining. Live CD8+ T cells sorted via flow cytometry were stained in PBS with MitoTracker Deep Red FM (Thermofisher, M22426) following the manufacturer's protocol. Cells were incubated with 500 nM MitoTracker for 15 minutes at room temperature. After staining, cells were washed once and immediately analyzed by the fluorescent coupled SMR.

Mass-based cell sorting. T cells were sorted based on buoyant mass measured by the SMR and observed by brightfield microscopy as they were controlled by standard pressure-driven fluidic components (**Supplementary Fig. 4**). Prior to sorting, cell concentrations were quantified utilizing a Coulter Counter (Beckman Inc.) and subsequently adjusted to a density of 100,000 cells/mL in PBS if measured concentration exceeded this value. The sorting parameters were established at a threshold of 7.5 pg for mouse T cells controlled by custom software coded in LabVIEW 2020 (National Instruments). Cells were sorted into 1.5 mL Eppendorf tubes, each filled with 35 uL of PBS+2%FBS, at a throughput of around 1,000 cells per hour. To maintain cell viability, all the T cell samples were preserved at 4 C before, during and after the sorting procedure.

Bulk RNA-sequencing. For bulk RNA-sequencing, naive CD8+ T cells were sorted by mass into heavy (>7.5 pg) and light (<7.5 pg) T cell populations. At least 800 cells were sorted per condition. Sorted cell samples were brought to a volume of 250 uL with PBS and then 750 uL of Trizol (Invitrogen, 10296010) was subsequently added. Samples were then incubated for 5 minutes at room temperature. Following incubation, samples were transferred to 2 mL maXtract high density tubes (Qiagen, 129056) and 200 uL of chloroform was added. Samples were then vigorously mixed at room temperature for 2 minutes. To separate phases, samples were centrifuged for 5 minutes at 4 C and 12000xg. The aqueous phase was collected and mixed 1:1 with 70% ethanol. Following this step, the RNeasy Plus Micro Kit (Qiagen, 74034) was followed per manufacturer's protocol starting at step 6. To briefly summarize the protocol, the RNA is collected in the RNeasy MinElute spin column, then washed with Buffer RW1, Buffer RPE, and 80% ethanol, and finally RNA is eluted in 14 uL of RNA-free water. After elution, RNA samples were stored at -80 C until they were sequenced.

Samples were sent to MIT BioMicroCenter for library prep and subsequent RNA sequencing. Nucleic acid was treated with DNase (NEB), purified using RNA SPRI beads, and quantified using an Agilent FemtoPulse. cDNA was generated using Takara SMART-Seq® v4 Ultra® Low Input RNA Kit for Sequencing and Singular libraries prepared using Illumina NexteraXT with modified amplification oligonucleotides containing Singular S1/S2 anchors instead of Illumina P5/P7 (DNAscript Syntax). Libraries were sequenced on a Singular G4 sequencer using 150nt paired end reads.

Raw sequencing reads were aligned to the mmu10 reference genome using STAR, and transcripts were quantified using featureCounts. Lowly expressed genes with fewer than 10 counts across more than 3 samples were filtered out. DESeq2 was used to normalize data and identify differentially expressed genes from the resulting count matrix. Genes with adjusted p values < 0.05 and absolute fold changes > 1.5 were considered significantly differentially expressed. The KEGGREST package was used to compile genes from relevant KEGG pathways for plotting with pheatmap. The set of mitochondrial genes was produced by selecting all genes beginning with the string "mt-".

Bulk T cell activation (>1 million T cells activated). Mouse CD8+ T cells were activated with plate bound anti-CD3 (10 ug/mL, clone 145-2C11, BioXCell) and anti-CD28 (2 ug/mL, clone 37.51, BioXCell) in a tissue culture treated 24 well plate. Cells were seeded at a concentration of 1 million per well in T cell activation media. T cell activation media used was composed of RPMI (Invitrogen, 11875085) supplemented with 10% FBS (Gibco, 10438-026), 1% P/S (Gibco, 15140-122), 1x NEAA (Gibco, 11140-050), 1 mM sodium pyruvate (Gibco, 11360-070), 55 uM 2-mercaptoethanol (Gibco, 21985-023), 1x ITS (Gibco, 41400-045), and 10ng/mL IL-2 (StemCell, 78081). Cells were then maintained in the incubator at 37 C for 28 hours. At the 28 hour time point, cells were washed from the plate and stained with Ki67 and fixable viability dye for sorting of live cells immediately followed with fluorescent coupled SMR measurements.

Low T cell count activation (<1000 T cells activated). T cells sorted by buoyant mass into light and heavy subpopulations were activated and expanded for 6 days. T cells were activated with Dynabeads Mouse T-activator CD3/CD28 for T-cell expansion and activation (GIBCO, 11456D). Cells were seeded with beads at a concentration of 200 cells per well with a 1:8 cell:bead ratio in the InSphero Akura 96 spheroid microplate (InSphero, CS-PB15). Once T cells, beads, and media were all added to the wells, the whole plate was centrifuged for 6 minutes at 600xg to promote cell and bead contact. After centrifugation, the supernatant was removed and T cell activation media was added (RPMI supplemented with 10% FBS, 1% P/S, 1x NEAA, 1mM sodium pyruvate, 55 uM 2-mercaptoethanol, 1x ITS, and 10ng/mL IL-2). The plate was then stored in the incubator at 37 C for 6 days. Wells were imaged daily and on the 6th day, cells were stained with FC Block (101302), eBioscience Fixable Viability Dye (APC-Cy7, 65-0865-14), Ki67 (FITC, 11-5698-80), CD279 (PD-1) (Super Bright 600, 63-9985-80), CD366 (Tim3) (BV421, 119723), IFNg (APC, 17-7311-81), CD137 (4-1BB) (PE, 12-1371-81), CD62L (APC, 17-0621-81), and Granzyme B (Pacific Blue, 515407) for analysis via flow cytometry.

Tumor conditioned media generation. KP-SIY cell line was grown at 37 °C and 5% CO_2 in standard DMEM medium (Sigma, D5796-500ML) supplemented with 10% FBS (Gibco, 10438-026), 1% penicillin/streptomycin (GIBCO, 15140-122), and 2 ug/mL puromycin (Sigma, P8833-25mg). Media was removed from the cells after 7 days of culture (3 days after confluency) and filtered with a 0.2 um filter to remove any remaining cells or debris. This media was stored at -80 C until the time of use. Media was thawed immediately before activation and mixed 1:9 with T cell activation media.

T cell activation imaging. Over the course of the 6 day T cell activation, wells were visualized daily on the Nikon Eclipse TS100 using a 4x objective. Brightfield images were captured using the FLIR Blackfly S Monochrome Camera (Edmund Optics, BFS-U3-04S2M-CS).

Tumor cell lines. Tumor cell lines, KP-SIY and MC-57-SIY, were cultured at 37C and 5% CO2 in DMEM (GIBCO) supplemented with 10% FBS (Atlanta Biologicals), 1% penicillin/streptomycin (GIBCO), and 1X HEPES (GIBCO). For tumor implantation, tumor cells were harvested by trypsinization (GIBCO), washed twice with 1X PBS (GIBCO), resuspended in PBS.

Mouse tumor models

KP-SIY. KP-SIY cells (2.5×10^5) were injected subcutaneously in the flank of 10 week old wildtype C57BL/6. Two weeks after injection, mice were euthanized via CO_2 asphyxiation. Tumors were dissected and minced in RPMI supplemented with 250 mg/mL Liberase (Sigma-Aldrich) and 50 mg/mL DNase (Sigma-Aldrich). Samples were then incubated at 37 C for 30 minutes and subsequently mashed through a 70 um filter to generate a single cell suspension. CD8+ T cells were enriched with the mouse CD8a+ T Cell Isolation Kit (Miltenyi, 130-104-075). The CD8 enriched sample was then stained with FC Block (101330), eBioscience Fixable Viability Dye (APC-Cy7, 65-0865-14), CD19 (APC-Cy7, 15530), NK1.1 (APC-Cy7, 108724), CD45 (APC, 103112), CD90.2 (Thy1.2) (BV421, 140327), CD8 (BV510, 100751), CD4 (AF488,100529), CD279 (PD-1) (PE-TR,109116), and CD366 (PE-Cy7, 25-5870-82) for fluorescent activated cell sorting of tumor infiltrating exhausted T cells.

MC-57-SIY. MC-57-SIY cells (1×10^6) were injected subcutaneously in the flank. Five weeks after MC-57-SIY injection, mice were euthanized via CO_2 asphyxiation. Spleen and inguinal lymph nodes were harvested and mashed through a 70 um filter. ACK lysing buffer (GIBCO) was used to lyse red blood cells in spleen samples (lysis performed for 2 minutes on ice, followed by 2 washes with PBS). CD8+ T cells were enriched with the mouse CD8a+ T Cell Isolation Kit (Miltenyi, 130-104-075). The CD8 enriched sample was then stained with FC Block (101330), eBioscience Fixable Viability Dye (APC-Cy7, 65-0865-14), CD19 (APC-Cy7, 15530), NK1.1 (APC-Cy7, 108724), CD45.1 (APC, 110714), CD45.2 (PE, 109807), CD90.2 (Thy1.2) (BV421, 140327), CD8 (BV510, 100751), CD4 (PerCP-Cy5.5, 100540), CD44 (AF488, 109116), and CD62L (BV785, 104440) for fluorescent activated cell sorting of central memory and effector memory CD8+ T cell subpopulations.

Flow cytometry. For flow cytometric analyses, cells were resuspended in staining buffer (Rockland, MB-086-0500) plus eBiosciences Fixable Viability Dye eFluor 780 and anti-CD16/CD32 and incubated at 4 C for 15 minutes. Cells were washed and then stained for surface proteins with fluorophore conjugated specific antibodies at 4 C for 30 min. If intracellular staining was required, eBioscience™ Intracellular Fixation & Permeabilization Buffer Set (Invitrogen, 88-8824-00) was used. Washed cells were resuspended in 100 uL of the fixation buffer and incubated in the dark at room temperature for 20 minutes. Cells were then washed twice in 1X Permabilization buffer. After completion of the washes, cells were resuspended in 100 uL of the permeabilization buffer with fluorophore conjugated specific antibodies and incubated for 20 minutes at room temperature in the dark. After a washing step, cells were immediately taken to flow cytometry for sorting.

Amnis Imagestream measurement of cell shape and fluorescence. To quantitatively evaluate light vs heavy T cells, sorted T cells were stained and imaged on the Amnis Imagestream. Images were collected using the duo channel brightfield setting. Cell parameters of both light and heavy were analyzed using Amnis IDEAs. Raw data were output and plotted using GraphPad Prism. Fluorescent gatings were collected based on single color controls and fluorescent-minus-one gatings.

Statistical analysis. The results are shown as mean ± standard error of the mean (SEM). To determine the statistical significance of the differences between the experimental groups two-tailed unpaired or paired Student's t tests, 2-way ANOVA tests were performed using the Prism 10 software (GraphPad), as indicated in each figure. Sample sizes were based on experience and experimental complexity, but no methods were used to determine normal distribution of the samples. Differences reached significance with p values < 0.05 (p values noted in figures). The figure captions contain the number of independent experiments or mice per group that were used in the respective experiments.

Reporting Summary

Further information on research design is available in the Nature Research Reporting Summary linked to this article.

Data availability

The authors declare that all data supporting the findings of this study are available within the paper and its Supplementary Information. Source data for the primary- sample figures are available.

Code availability

Custom SMR data processing and sequencing analysis code is available in the supplemental information.

References

1. Sallusto, F., Lanzavecchia, A., Araki, K. & Ahmed, R. From vaccines to memory and back. Immunity 33, 451–463 (2010).
2. Zinkernagel, R. M. & Doherty, P. C. MHC-restricted cytotoxic T cells: studies on the biological role of polymorphic major transplantation antigens determining T-cell restriction-specificity, function, and responsiveness. Adv. Immunol. 27, 51–177 (1979).
3. Ribas, A. & Wolchok, J. D. Cancer immunotherapy using checkpoint blockade. Science 359, 1350–1355 (2018).
4. Dijkstra, K. K. et al. Generation of Tumor-Reactive T Cells by Co-culture of Peripheral Blood Lymphocytes and Tumor Organoids. Cell 174, 1586–1598.e12 (2018).
5. Restifo, N. P., Dudley, M. E. & Rosenberg, S. A. Adoptive immunotherapy for cancer: harnessing the T cell response. Nat. Rev. Immunol. 12, 269–281 (2012).
6. Xia, A., Zhang, Y., Xu, J., Yin, T. & Lu, X.-J. T Cell Dysfunction in Cancer Immunity and Immunotherapy. Front. Immunol. 10, 1719 (2019).
7. Wherry, E. J. & Kurachi, M. Molecular and cellular insights into T cell exhaustion. Nat. Rev. Immunol. 15, 486–499 (2015).
8. Sade-Feldman, M. et al. Defining T Cell States Associated with Response to Checkpoint Immunotherapy in Melanoma. Cell 175, 998–1013.e20 (2018).
9. Burg, T. P. et al. Weighing of biomolecules, single cells and single nanoparticles in fluid. Nature 446, 1066–1069 (2007).
10. Olcum, S., Cermak, N., Wasserman, S. C. & Manalis, S. R. High-speed multiple-mode mass-sensing resolves dynamic nanoscale mass distributions. Nat. Commun. 6, 7070 (2015).
11. Stockslager, M. A. et al. Functional drug susceptibility testing using single-cell mass predicts treatment outcome in patient-derived cancer neurosphere models. Cell Rep. 37, 109788 (2021).
12. Kimmerling, R. J. et al. Linking single-cell measurements of mass, growth rate, and gene expression. Genome Biol. 19, 207 (2018).
13. Cermak, N. et al. High-throughput measurement of single-cell growth rates using serial microfluidic mass sensor arrays. Nat. Biotechnol. 34, 1052–1059 (2016).
14. Latimer, P. Light scattering vs. microscopy for measuring average cell size and shape. Biophys. J. 27, 117–126 (1979).
15. Wu, T. et al. Cell Granularity Reflects Immune Cell Function and Enables Selection of Lymphocytes with Superior Attributes for Immunotherapy. Adv. Sci. 10, e2302175 (2023).
16. Miettinen, T. P., Ly, K. S., Lam, A. & Manalis, S. R. Single-cell monitoring of dry mass and dry mass density reveals exocytosis of cellular dry contents in mitosis. Elife 11, (2022).
17. Feijó Delgado, F. et al. Intracellular water exchange for measuring the dry mass, water mass and changes in chemical composition of living cells. PLoS One 8, e67590 (2013).
18. Nakajima, Y., Chamoto, K., Oura, T. & Honjo, T. Critical role of the CD44CD62L CD8 T cell subset in restoring antitumor immunity in aged mice. Proc. Natl. Acad. Sci. U. S. A. 118, (2021).
19. Sprent, J. & Surh, C. D. Normal T cell homeostasis: the conversion of naive cells into memory-phenotype cells. Nat. Immunol. 12, 478–484 (2011).
20. Jameson, S. C. & Masopust, D. Diversity in T cell memory: an embarrassment of riches. Immunity 31, 859–871 (2009).
21. Wolf, T. et al. Dynamics in protein translation sustaining T cell preparedness. Nat. Immunol. 21, 927–937 (2020).
22. Riddell, S. R. & Greenberg, P. D. The use of anti-CD3 and anti-CD28 monoclonal antibodies to clone and expand human antigen-specific T cells. J. Immunol. Methods 128, 189–201 (1990).
23. Appay, V., Douek, D. C. & Price, D. A. CD8+ T cell efficacy in vaccination and disease. Nat. Med. 14, 623–628 (2008).
24. Zhou, R., Yazdi, A. S., Menu, P. & Tschopp, J. A role for mitochondria in NLRP3 inflammasome activation. Nature 469, 221–225 (2010).
25. Zhang, L. et al. Mitochondria dysfunction in CD8+ T cells as an important contributing factor for cancer development and a potential target for cancer treatment: a review. J. Exp. Clin. Cancer Res. 41, 227 (2022).
26. Van der Windt, G. J. W. et al. Mitochondrial respiratory capacity is a critical regulator of CD8+ T cell memory development. Immunity 36, 68–78 (2012).
27. Vardhana, S. A. et al. Impaired mitochondrial oxidative phosphorylation limits the self-renewal of T cells exposed to persistent antigen. Nat. Immunol. 21, 1022–1033 (2020).
28. Singh, N., Perazzelli, J., Grupp, S. A. & Barrett, D. M. Early memory phenotypes drive T cell proliferation in patients with pediatric malignancies. Sci. Transl. Med. 8, 320ra3 (2016).
29. Wu, H. et al. Mitochondrial dysfunction promotes the transition of precursor to terminally exhausted T cells through HIF-1α-mediated glycolytic reprogramming. Nat. Commun. 14, 1–18 (2023).

30. Yu, Y.-R. et al. Disturbed mitochondrial dynamics in CD8+ TILs reinforce T cell exhaustion. Nat. Immunol. 21, 1540–1551 (2020).
31. Scharping, N. E. et al. Mitochondrial stress induced by continuous stimulation under hypoxia rapidly drives T cell exhaustion. Nat. Immunol. 22, 205–215 (2021).
32. Yun, S. J. et al. Regulation of TIM-3 expression in a human T cell line by tumor-conditioned media and cyclic AMP-dependent signaling. Mol. Immunol. 105, 224–232 (2019).
33. LaFave, L. M. et al. Epigenomic State Transitions Characterize Tumor Progression in Mouse Lung Adenocarcinoma. Cancer Cell 38, 212–228.e13 (2020).
34. Cheung, A. F., DuPage, M. J. P., Dong, H. K., Chen, J. & Jacks, T. Regulated Expression of a Tumor-Associated Antigen Reveals Multiple Levels of T-Cell Tolerance in a Mouse Model of Lung Cancer. Cancer Res. 68, 9459–9468 (2008).
35. Horton, B. L. et al. Lack of CD8 T cell effector differentiation during priming mediates checkpoint blockade resistance in non-small cell lung cancer. Sci Immunol 6, eabi8800 (2021).
36. Kim, A. M. J., Nemeth, M. R. & Lim, S.-O. 4-1BB: A promising target for cancer immunotherapy. Front. Oncol. 12, 968360 (2022).
37. Sallusto, F., Geginat, J. & Lanzavecchia, A. Central Memory and Effector Memory T Cell Subsets: Function, Generation, and Maintenance. Annu. Rev. Immunol. 22, 745–763 (2004).
38. Pan, M. & Li, B. T cell receptor convergence is an indicator of antigen-specific T cell response in cancer immunotherapies. (2022) doi:10.7554/eLife.81952.
39. Spranger, S., Dai, D., Horton, B. & Gajewski, T. F. Tumor-Residing Batf3 Dendritic Cells Are Required for Effector T Cell Trafficking and Adoptive T Cell Therapy. Cancer Cell 31, 711–723.e4 (2017).
40. Spiotto, M. T. et al. Increasing tumor antigen expression overcomes 'ignorance' to solid tumors via cross presentation by bone marrow-derived stromal cells. Immunity 17, 737–747 (2002).
41. Huh, D. et al. Gravity-driven microfluidic particle sorting device with hydrodynamic separation amplification. Anal. Chem. 79, 1369–1376 (2007).
42. Roda, B. et al. Human lymphocyte sorting by gravitational field-flow fractionation. Anal. Bioanal. Chem. 392, 137–145 (2008).

Acknowledgements
We thank the Brigham and Women's Hospital Specimen Bank for providing human donor PBMC collar samples, and for Dr. Lydie Debaize, Dr. Mark Murakami, coordination. We thank Dr. Leyuan Ma, Dr. Kewen Lei and Dr. Darrell Irvine for helpful discussion in T cell activation, flow cytometry, and mouse work. We thank Kevin Yang for discussion and for helping the schematics in the figures. We thank the laboratory of Tyler Jacks for providing C57BL/6; 129/Sv mixed background mice. Some schematics presented in this work were created with BioRender.com.

Funding
S.R.M. discloses support for the research described in this study from D.K. Ludwig Fund for Cancer Research, MIT Center for Precision Cancer Medicine and Stand Up to Cancer (SU2C) Convergence Program 3.1416.

Author contributions
Y.Z., J.Y, and S.R.M. conceptualized the study. Y.Z. designed and built the sorting device with assistance from S.R.M. For in vitro experiments, J.Y, S.M.D, T.U. and Y.Z designed and carried out the experiments. For in vivo experiments, T.D., S.M.D., J.Y., Y.Z designed and carried out the experiments. G.L.Y. analyzed the RNA-sequencing data, J.Y., Y.Z assisted the analysis. J.Y. Y.Z and S.M.D wrote the manuscript with contributions from S.R.M. All authors reviewed and approved the manuscript.

Competing interests
S.R.M. is a founder of Travera and Affinity Biosensors. J.Y. is a founder of Stacks to the Future LLC. The other authors declare no competing interests.

Supplementary Information

Contents

Supplemental Note 1: Relationship between cellular buoyant mass and dry mass
Supplementary Fig.1: Separating CD8 T cells by light scattering
Supplementary Fig.2: Amnis Imagestream brightfield images of heavy and light T cells
Supplementary Fig.3: Isolating CD8+ T cells using flow cytometry
Supplementary Fig.4: Pipeline for mass-based SMR single cell sorting
Supplementary Fig.5: Mass-based SMR sorting system has high accuracy
Supplementary Fig.6: Differential gene expression of light and heavy T cells
Supplementary Fig.7: Gene set enrichment analysis of light and heavy T cells
Supplementary Fig.8: Gene pathway analysis
Supplementary Fig.9: Principal component analysis of light and heavy T cells mRNA expression
Supplementary Fig.10: CD3/CD28 Dynabeads T cell activation
Supplementary Fig.11: Mass profile of activated light and heavy T cells
Supplementary Fig.12: Light and heavy activated T cells Amnis Imagestream gating
Supplementary Fig.13: CD3/CD28 Dynabeads T cell activation in tumor conditioned media
Supplementary Fig.14: Tumor conditioned media activated T cells Amnis Imagestream gating
Supplementary Fig.15: Isolating exhausted CD8+ T cells using flow cytometry
Supplementary Fig.16: Isolating central and effector memory T cells using flow cytometry

Supplemental Note 1: Relationship between cellular buoyant mass and dry mass

Cell buoyant mass, m_b, includes a component from the dry material and another from the intracellular water content as given by

$$m_b = m_{dry}(1 - \frac{\rho_{fluid}}{\rho_{dry}}) + V_{iw}(\rho_{iw} - \rho_{fluid}) \quad (1)$$

where ρ_{fluid} is the fluid density, m_{dry} and ρ_{dry} are the mass and density of the cell's dry materials, and V_{iw} and ρ_{iw} are the volume and density of the exchangeable water content. When cells are in media where the density is close to that of water ($\rho_{iw} \approx \rho_{fluid}$), the buoyant mass depends on only dry mass and dry density

$$m_b = m_{dry}(1 - \frac{\rho_{fluid}}{\rho_{dry}}) \quad (2)$$

In our measurements, cells were suspended in 1X PBS ($\rho_{fluid} = 1.005\ g \cdot cm^{-3}$). Theoretically, when the dry density in equation (2) is constant across both light and heavy populations ($\rho_{dry} \approx 1.4\ g \cdot cm^{-3}$ as previously reported[1]), the buoyant mass is linearly correlated with the dry mass with a constant slope $k = 1/(1 - \frac{\rho_{fluid}}{\rho_{dry}}) \approx 3.5$. Based on our measurements, linear regression between buoyant mass and dry mass of the heavy population is consistent with this theoretical estimate while the light population does not match as well (**Supplementary Fig. Note1**). These calculations indicate that light and heavy T cells have different dry densities. Moreover, this observation appears in both human and mouse samples.

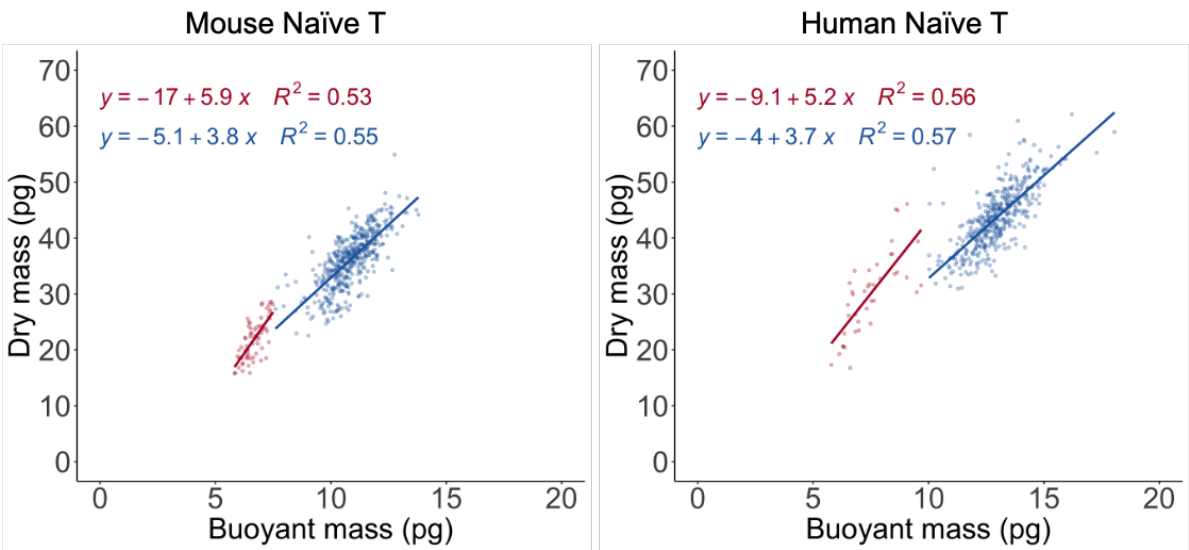

Supplementary Fig. Note1 | Relationship between cellular buoyant mass and dry mass. Buoyant mass and dry mass of mouse and human naïve T cells. Light cells are represented in red while heavy ones in blue. Lines in the graphs represent the linear regression between buoyant mass and dry mass of each population.

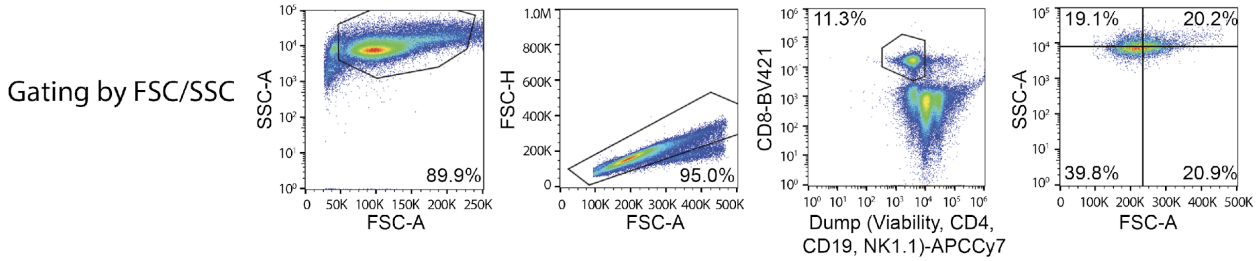

Supplementary Fig.1 | Separating CD8 T cells by light scattering. Representative gating strategy to sort CD8 T cells by light scattering. Samples from Q2 (i.e. High SSC-A high FSC-A) and Q4 (low SSC-A low FSC-A) were collected and measured with the SMR as shown in **Fig. 1e**.

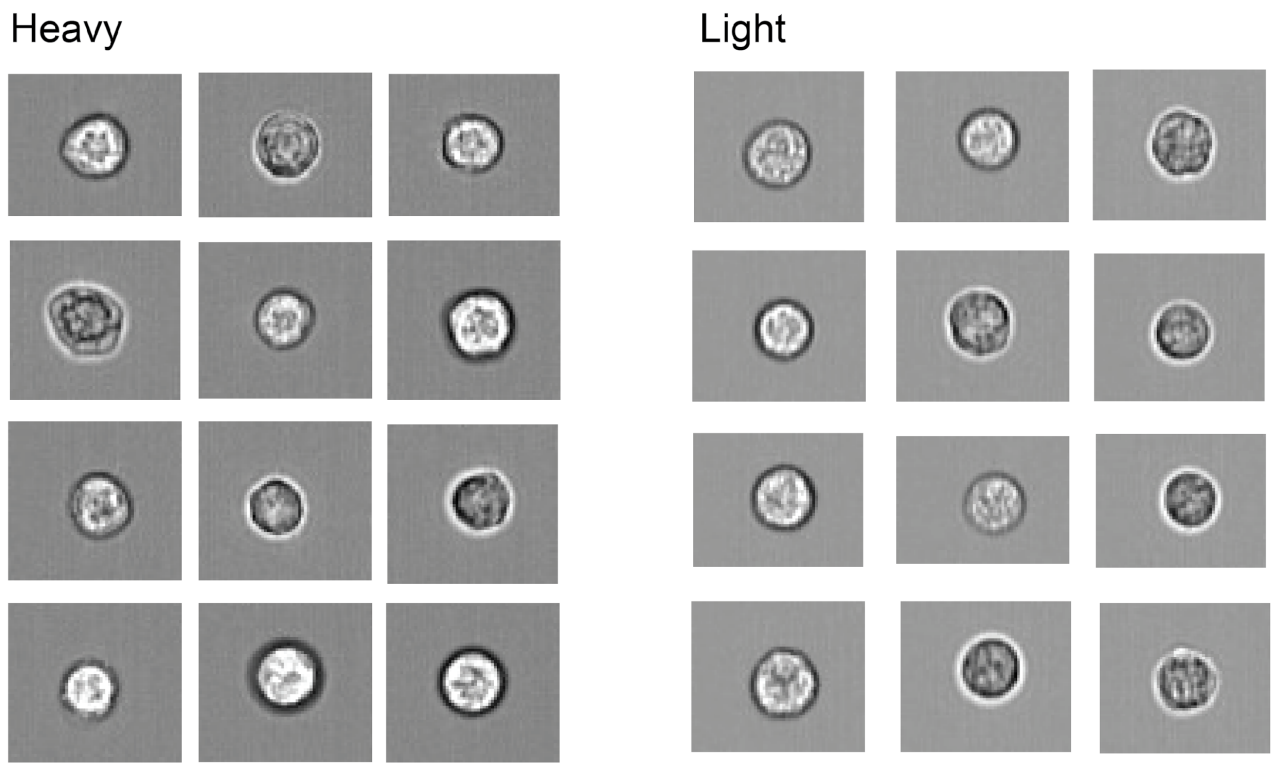

Supplementary Fig.2 | Amnis Imagestream brightfield images of heavy and light T cells.
Representative brightfield image from the Amnis Imagestream of heavy and light mouse spleen CD8+ T cells.

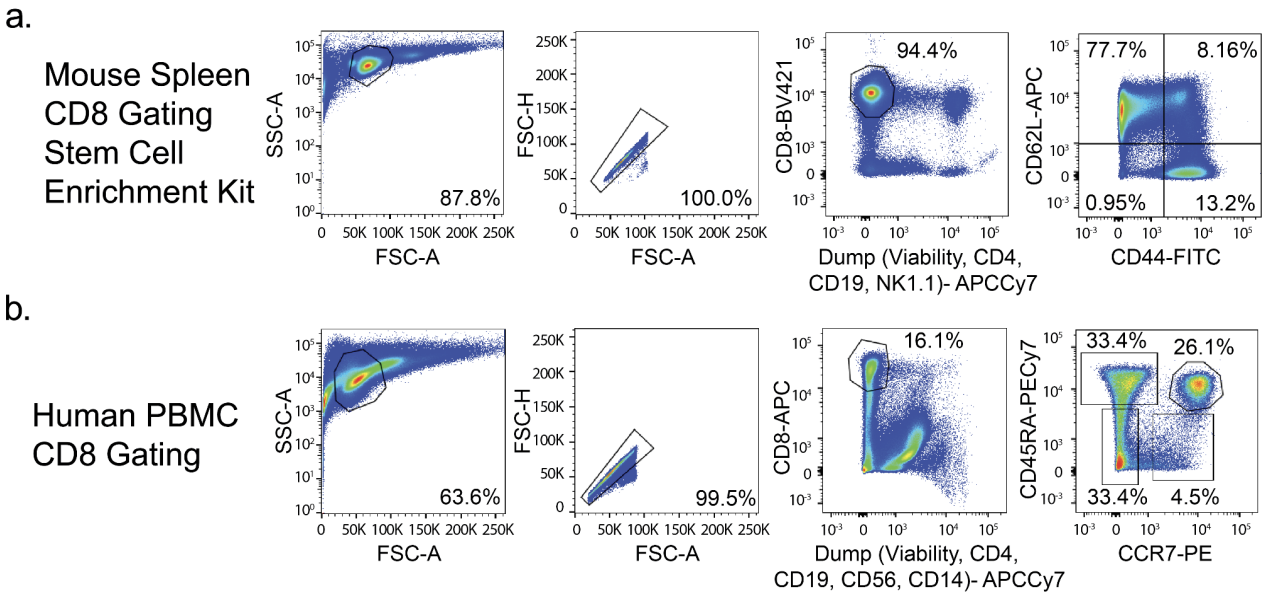

Supplementary Fig.3 | Isolating CD8+ T cells using flow cytometry. a, Representative gating strategy to identify and sort naive (CD62L+, CD44-), central memory (CD62L+, CD44-), and effector memory (CD62L-, CD44+) CD8+ T cell subpopulations from healthy mouse spleen samples. **b,** Representative gating strategy to identify and sort naive (CD4RA+, CCR7+), central memory (CD45RA-, CCR7+), effector memory (CD45RA-, CCR7-), and effector memory re-expressing CD45RA (CD45RA+, CCR7-) CD8+ T cells from donor human PBMC samples.

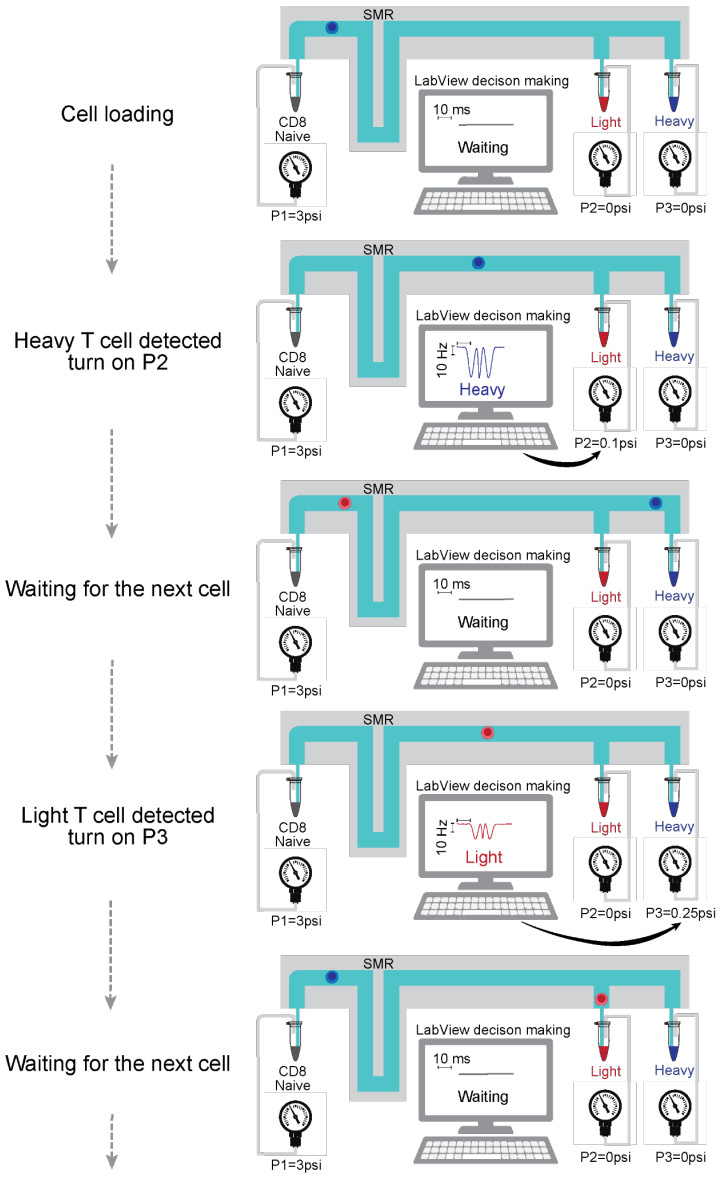

Supplementary Fig.4 | Pipeline for mass-based SMR single cell sorting. T cells (naive or CD8) are loaded onto the system with positive pressure from regulator 1 (P1). As the cells flow through the cantilever on SMR, the mass of the cell is recorded as frequency shift (Hz). A decision is made in LabVIEW based on the frequency shift and pre-set thresholds to control the subsequent regulators P2 and P3. For example, a mouse T cell heavier than 12.5 Hz is considered heavy and will trigger pressure regulator P2 to direct the cell into the heavy collector. On the contrary, a light cell will trigger regulator P3 to direct the cells into the light collector. The system allows only one cell in the fluidic path at any given time to ensure sorting accuracy (**Supplementary Fig.5**). The process repeats for each cell automatically. Cells are sorted at a rate of about 1000 cells per hour.

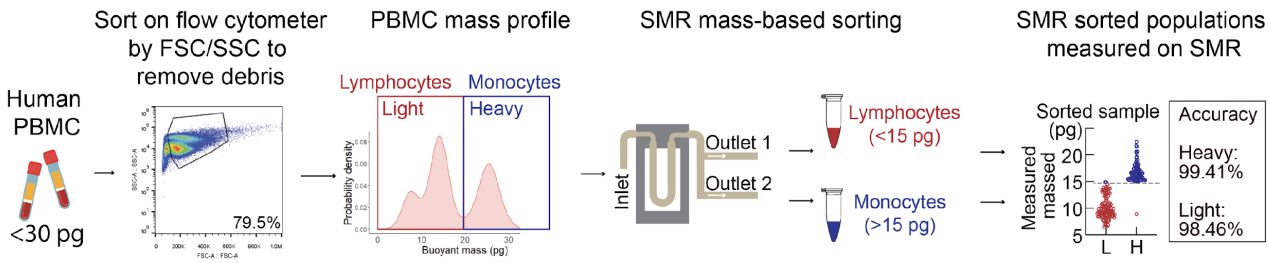

Supplementary Fig.5 | Mass-based SMR sorting system has high accuracy. A PBMC sample was used to test sorting accuracy. Lymphocytes and monocytes were collected from a human PBMC sample through FSC-SSC sorting on flow cytometry. Monocytes are distinctly heavier than lymphocytes. We sorted monocytes and lymphocytes based on mass. The sorted samples were then measured on SMR to evaluate the sorting accuracy. Accuracy is defined as the percentage of cells in the light (or heavy) compartment that is measured to be light. The heavy compartment has an accuracy of 99.41% and the light 98.46%.

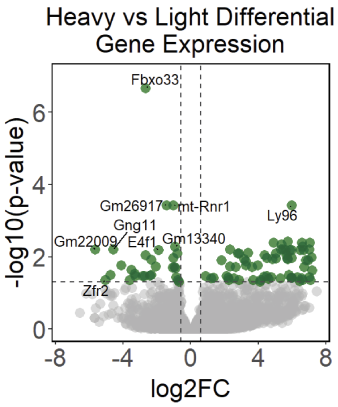

Supplementary Fig.6 | Differential gene expression of light and heavy T cells. Volcano plot of heavy vs. light differential gene expression. Heavy cells were used as reference and fold change numbers represent light cells mRNA expression levels compared to heavy.

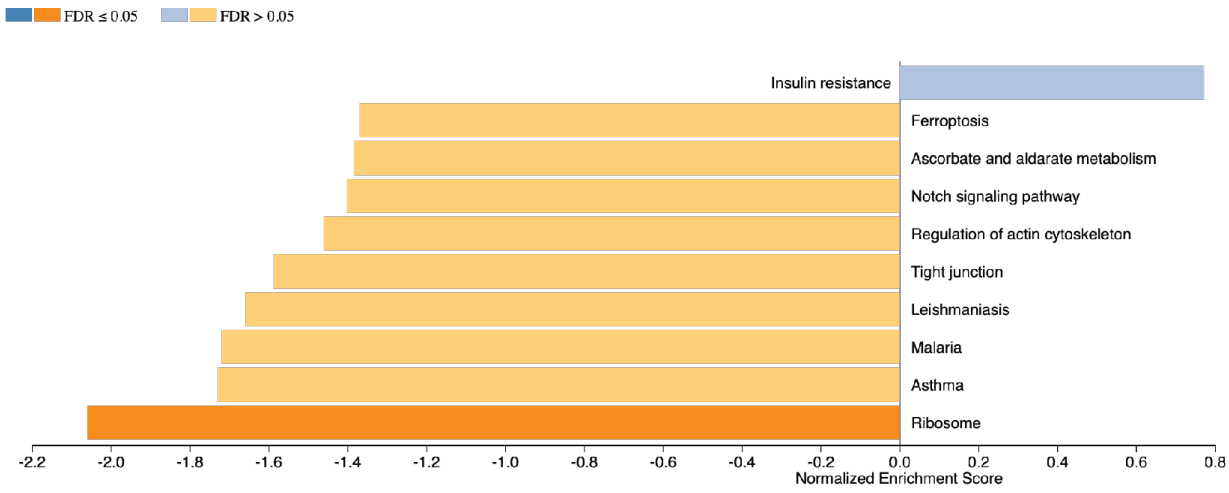

Supplementary Fig.7 | Gene set enrichment analysis of light and heavy T cells. KEGG gene set enrichment analysis was performed to compare light and heavy T cells. Heavy cells were used as reference and enrichment scores represent light cells mRNA expression levels compared to heavy.

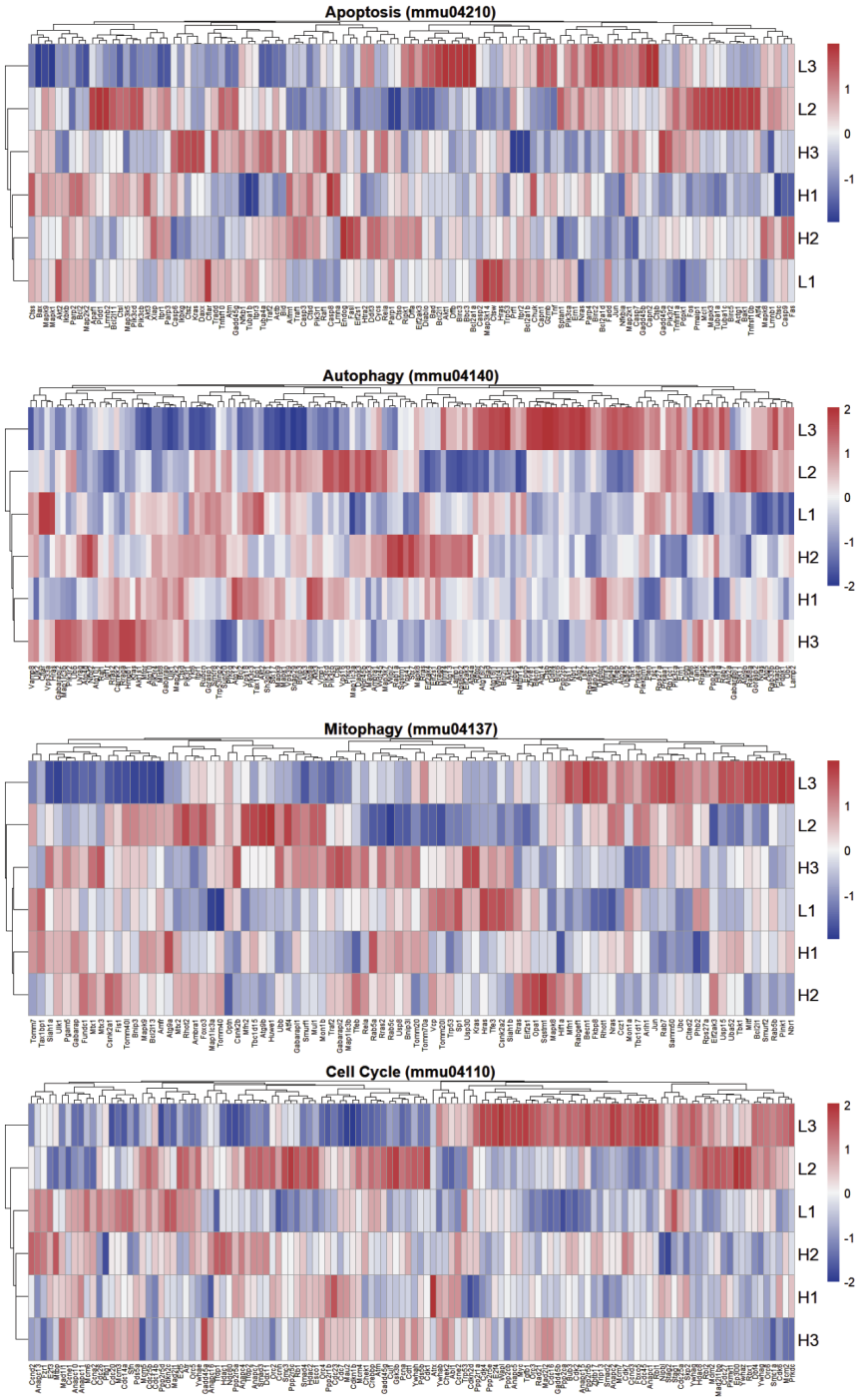

Supplementary Fig.8 | Gene pathway analysis. Heatmap visualization of genes related to pathways of interest. Pathways analyzed are **a,** apoptosis, **b,** autophagy, **c,** mitophagy, and **d,** cell cycle.

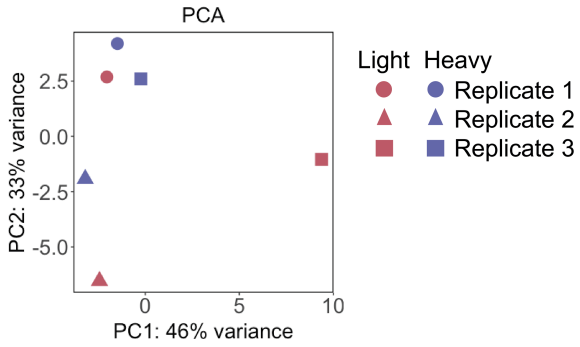

Supplementary Fig.9 | Principal component analysis of light and heavy T cells mRNA expression. Principal component analysis on heavy and light T cells. Shapes depict different replicates and color depicts buoyant mass.

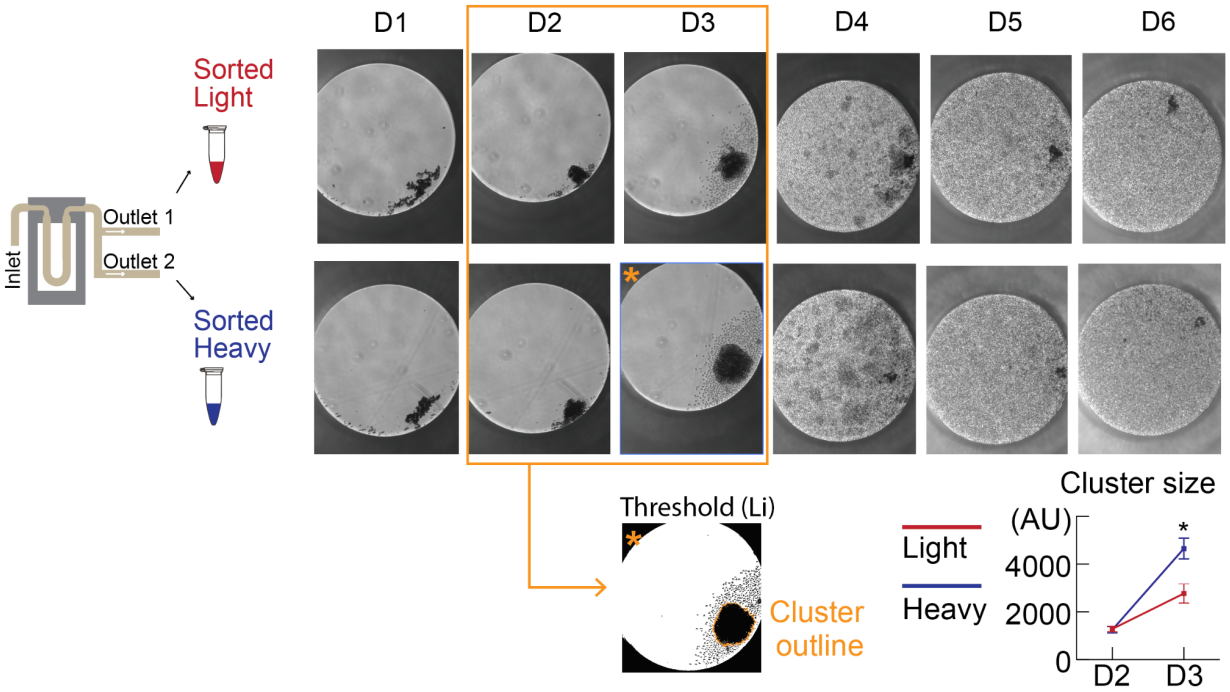

Supplementary Fig.10 | CD3/CD28 Dynabeads T cell activation. T cells sorted by mass were activated for 6 days and imaged daily. A cluster starts to form on day 1. Importantly there is no proliferation so the cluster is formed by T cells migrating and carrying the beads together (data not shown). The cluster grows in the following days, due to both enlargement of T cells during activation and proliferation. Images on day 5 and 6 show that the wells are confluent with T cells. Analysis of cluster size was performed on days 2 and 3. Li thresholding in ImageJ is used to identify the cluster so that cluster area can be calculated. An example of the cluster outline is shown in orange and the image used for analysis is indicated with a star.

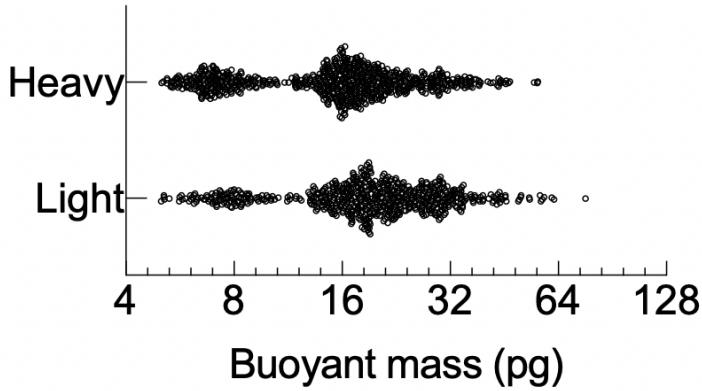

Supplementary Fig.11 | Mass profile of activated light and heavy T cells. CD8+ T cells sorted by mass into light and heavy bins were independently activated and subsequently measured on the SMR after 6 days.

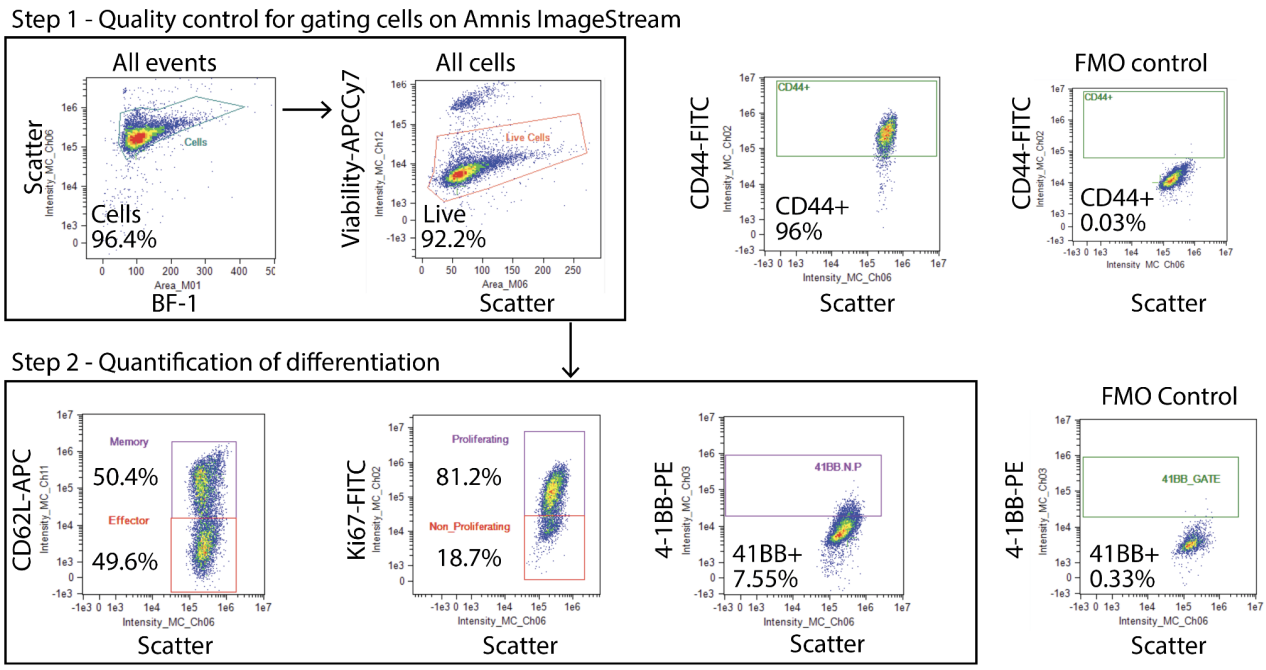

Supplementary Fig.12 | Light and heavy activated T cells Amnis Imagestream gating. Representative gating strategy to identify differentiated CD8+ T cell subtypes from activated light and heavyT cells using the Amnis Imagestream.

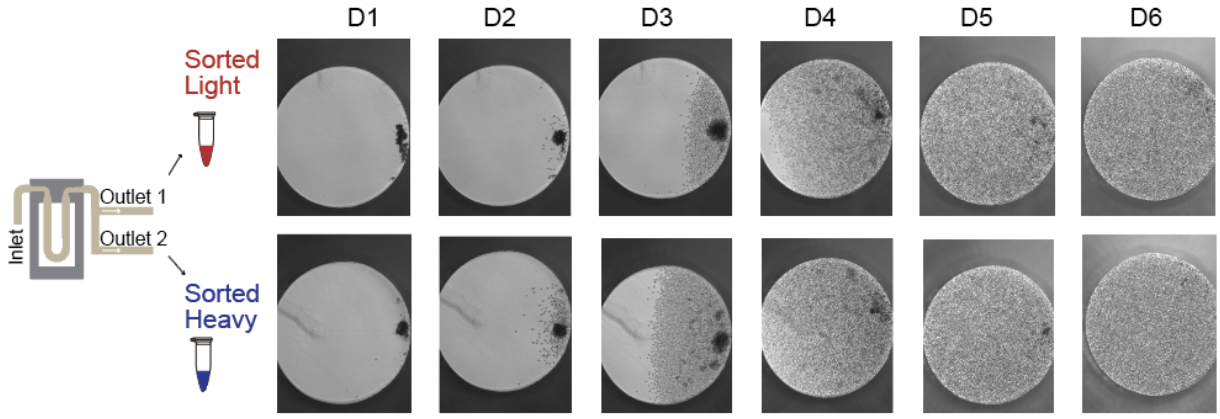

Supplementary Fig.13 | CD3/CD28 Dynabeads T cell activation in tumor conditioned media. T cells sorted by mass were activated in the presence of 10% tumor conditioned media for 6 days and imaged daily. Similar to activation without tumor conditioned media, clusters start to form on day 1. Cluster grows in the following days, due to both enlargement of T cells during activation and proliferation. Images on day 5 and 6 are confluent with T cells.

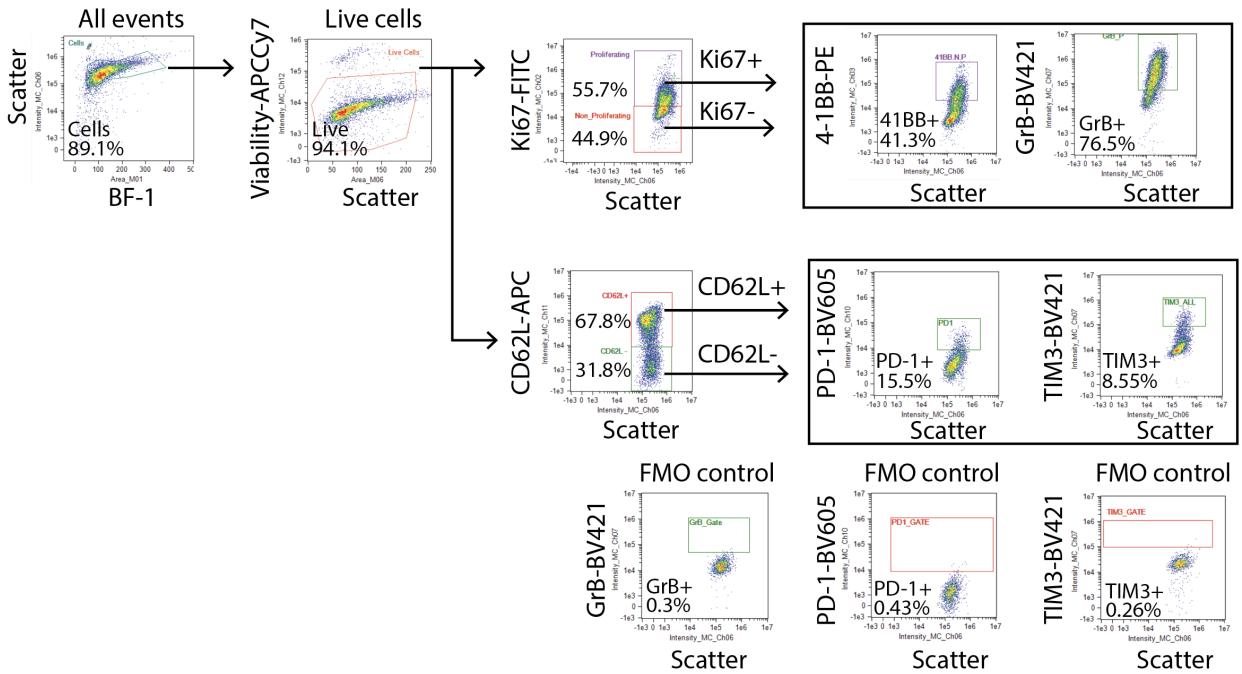

Supplementary Fig.14 | Tumor conditioned media activated T cells Amnis Imagestream gating. Representative gating strategy to identify differentiated CD8+ T cell subtypes from T cells activated in tumor conditioned media using the Amnis Imagestream.

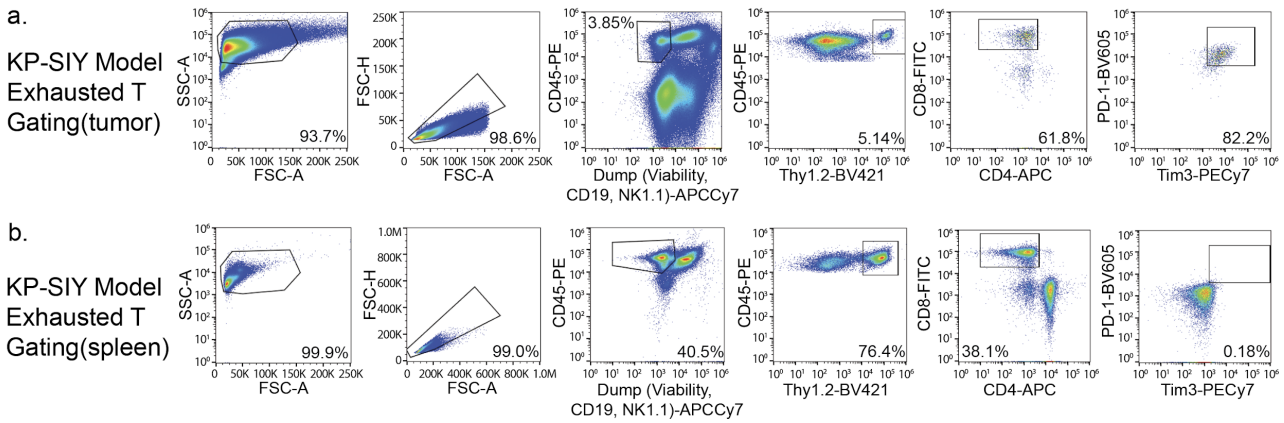

Supplementary Fig.15 | Isolating exhausted CD8+ T cells using flow cytometry. a, Representative gating strategy to identify and sort exhausted T cells from KP-SIY mouse tumors. **b,** Representative gating strategy on a KP-SIY mouse spleen to identify exhausted T cell gate.

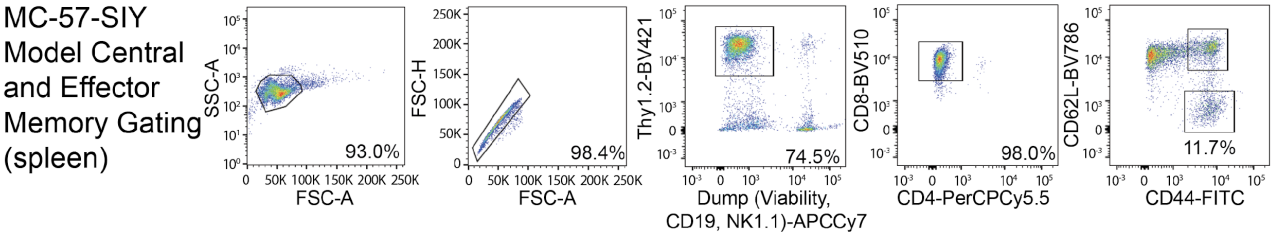

Supplementary Fig.16 | Isolating central and effector memory T cells using flow cytometry. Representative gating strategy to identify and sort central memory (CD62L+, CD44+) and effector memory (CD62L-, CD44+) CD8+ T cells from mouse spleens from mice that rejected MC-57-SIY tumors.

Reference

1. Miettinen, T. P., Ly, K. S., Lam, A. & Manalis, S. R. Single-cell monitoring of dry mass and dry mass density reveals exocytosis of cellular dry contents in mitosis. Elife 11, (2022).